Modelling of in-plane seismic behaviour of one-way steel or timber jack arch floors in existing buildings. Application to the Eixample district of Barcelona

Sara Dimovska[a] *, Savvas Saloustros [a,b], Luca Pelà[a] and Pere Roca[a]

[a] Universitat Politècnica de Catalunya (UPC-BarcelonaTech), Barcelona School of Civil Engineering (ETSECCPB), Department of Civil and Environmental Engineering (DECA), Jordi Girona 1-3, 08034 Barcelona, Spain.

[b] Laboratory of Earthquake Engineering and Structural Dynamics (EESD), School of Architecture, Civil and Environmental Engineering (ENAC), École Polytechnique Fédérale de Lausanne (EPFL), EPFL ENAC IIC EESD, GC B2 495, Station 18, 1015, Lausanne, Switzerland

Abstract – The type of floor system has a decisive role in the seismic performance of unreinforced masonry buildings. The in-plane stiffness of the floors has to be adequately represented in the numerical modelling of existing buildings, as it can influence their seismic capacity. This paper investigates the seismic behaviour of one-way arch floor systems composed of steel or timber beams, and ceramic tile vaults. The main objective of the research is to provide a numerical procedure for the simplified modelling of jack

* Corresponding author.

E-mail addresses: sara.dimovska@upc.edu (Sara Dimovska), savvas.saloustros@epfl.ch (Savvas Saloustros), luca.pela@upc.edu (Luca Pelà), pere.roca.fabregat@upc.edu (Pere Roca).

arch floor systems in the seismic assessment of unreinforced masonry buildings. The presented approach aims to provide values for the orthotropic properties of simplified floor models composed of elastic 2D shell elements. The orthotropic elastic properties are computed and calibrated by means of comparisons with detailed 3D nonlinear models of the floors. The case study is a multi-storey existing masonry building of the historical "Eixample" district in Barcelona, which includes one-way arch floor systems. The Finite Element Method has been used for the numerical simulation of the seismic performance through nonlinear static (pushover) analyses. The results of the study contribute to a better understanding of the effect of the behaviour of one-way floors with steel or timber beams and tile vaults on the seismic response of masonry buildings. This work provides indicative values for the proper modelling of these particular floor slabs. The proposed methodology is also applicable to the numerical simulation of any other one-way floor system.

Keywords: One-way Floor; Orthotropic Floor; Steel Beam; Timber Beam; Tile Vault; In-plane Stiffness; Unreinforced Masonry Building; Finite Element Analysis; Pushover Analysis; Seismic Vulnerability.

Highlights:

- Novel method for simplified 2D shell modelling of one-way jack arch floors
- 2D elastic orthotropic shell properties are calibrated via an iterative procedure
- Calibration based on comparisons with detailed nonlinear 3D floor modelling
- Application to timber/steel and tile vault floors of Eixample district, Barcelona
- Seismic performance analysis of an Eixample building with two different floors

1. Introduction

The response of unreinforced masonry (URM) structures under horizontal loading depends significantly on the in-plane stiffness of the diaphragms [1–3]. The existence of a flexible diaphragm may result in a lack of a box behaviour and in an increase of the seismic vulnerability [4]. The seismic vulnerability of a typical URM building can be affected by many parameters, such as material properties, plan distribution and regularity, in-plane stiffness of the horizontal diaphragms, and lack of connections between the lateral load bearing and horizontal elements [5,6]. Therefore, the flexibility of the floors can play an important role in the seismic performance of URM buildings. This point highlights the importance of estimating and considering in a realistic way the in-plane stiffness of floors in the seismic assessment of existing URM buildings.

The influence of deformable wooden floors on the seismic performance of unreinforced masonry buildings has been investigated, both at experimental and numerical level [6–10]. Additionally, international guidelines on seismic rehabilitation of buildings [11] provide some reference values for the shear stiffness of different flexible timber floors, and propose some analytical procedures for the evaluation of their in-plane stiffness [12]. However, there is scarce information regarding the in-plane behaviour of floor systems composed of timber beams (with round or squared section) or steel beams and ceramic vaults. These one-way floor slabs, called jack arch floors, are very common in many historical and existing buildings of the Mediterranean countries, and especially in the eastern coast of Spain [13,14]. Only a few studies, focusing on Iranian masonry or steel buildings,

have contributed to the evaluation of the shear stiffness and the seismic behaviour of this type of floor slabs [15–19].

This work investigates the in-plane stiffness of typical one-way floors in order to assess its effect on the seismic behaviour of URM buildings. The historic district of Barcelona called *Eixample* (meaning expansion or enlargement in Catalan) is the case study of this work, as the seismic response of a typical six-storey URM building is evaluated. Most of the buildings of the Eixample district are URM structures with slender walls and particular floor systems made of jack arches with steel or timber beams. These buildings were designed only for vertical static loads, without any regard for seismic requirements. The global seismic behaviour of these buildings was investigated during the past years [20–22], as they are highly vulnerable to seismic actions even in a region with a low to moderate hazard such as Barcelona.

The paper proposes a numerical procedure in order to define the orthotropic material properties for the modelling of one-way floors composed of beams (steel or timber) and ceramic tile vaults. This study aims to identify the influence of the floor deformability on the seismic response of URM buildings. In order to properly model the behaviour of the jack arch floors, 3D solid and 2D shell finite element models have been prepared for computing the elastic orthotropic properties of the composite floor system, by matching their effective stiffness with an iterative procedure. Subsequently, the seismic assessment of an existing URM building has been carried out by means of the Finite Element Method (FEM). Nonlinear static analyses have been performed in order to assess the seismic performance of the building modelled with the different one-way floor systems.

The primary objectives of this study are the following ones: 1) to present a general numerical procedure for evaluating and simulating the in-plane stiffness of the jack arch floors; 2) to provide values for the in-plane orthotropic elastic properties of two specific one-way floor systems; 3) to evaluate the effect of the behaviour of the floor system on the seismic response of a typical URM building of the Eixample district of Barcelona.

The paper is composed of seven sections. After the Introduction, Section 2 presents the main characteristics of one-way floor systems composed of steel or timber beams, and ceramic tile vaults, including also the historical survey of those existing in the URM buildings of the Eixample district of Barcelona. Section 3 and Section 4 describe the numerical FEM model of the URM Eixample building, and the FEM models of the jack arch floors with details on the material properties used in them, respectively. Section 5 presents the numerical procedure for the estimation of the in-plane orthotropic elastic properties of the two floor systems. Section 6 contains the interpretation of the results for the push-over analyses performed in order to study the influence of the typical floor systems. Finally, Section 7 presents the conclusions of this research.

2. Characteristics of one-way steel or timber jack arch floors

Jack arch floors are one-way floor systems composed of steel or timber beams and ceramic tile vaults that can be found in many industrial and urban buildings in Europe, as well as in several countries of the world. According to FEMA 356 [23], this floor system is considered as an archaic diaphragm composed of shallow brick arches that span between steel beams.

This specific one-way floor system with timber or steel beams had been a common horizontal structural system in the eastern coast of Spain since the 15th century until the middle of the 20th century [24]. They are present in many historical and existing buildings and represent a main feature of the architecture of this area of the Mediterranean. These particular floors have evolved during the years by the adoption of different materials and diverse construction techniques, resulting in floors of timber, steel elements, reinforced concrete or precast concrete. Figure 1 shows different configurations of the jack arch floors.

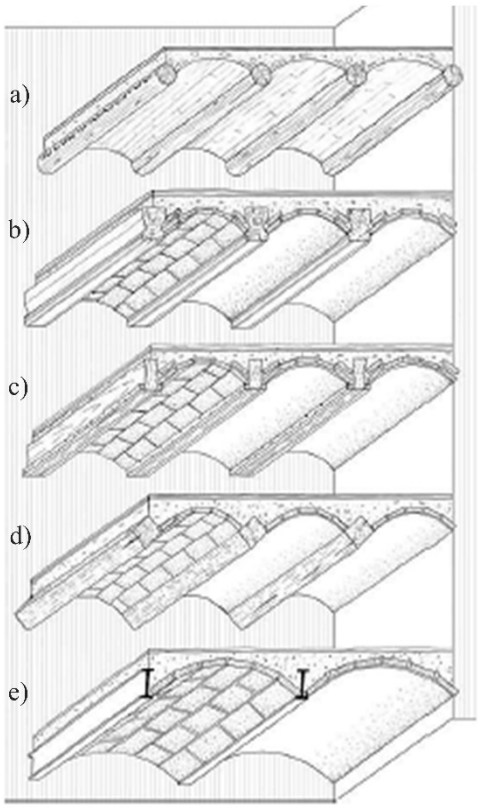

Figure 1 - Different configurations of jack arch floor in axonometric view: a) timber beams with round section (debarked trunk of tree) and plaster conglomerate vaults; b) timber beams with rectangular section and segmental barrel vaults; c) timber joists with two side battens nailed used for supporting the ceramic

tile vaults; d) squared timber joists (placed with a rotation of 45°) and tile vaults; e) steel I profiled beams with ceramic tile vaults (Figure adapted from Diodato et al. [14]).

Initially, the jack arch floors were composed of timber beams (with round or squared section) and segmental vaults made of flat tiles or poured plaster conglomerate (Figure 1a). This floor system became very popular because it allowed a simple construction of a light weighted structure with a reduced amount of wood [14].

According to Maheri and Rahmani [15], the jack arch floor with steel beams was developed in the post-industrial British revolution at the end of 19th century. This solution was extensively used to cover large floor areas in factories, warehouses and other industrial buildings. Later, this floor slab technique was adopted in Eastern Europe as well as in the Middle East and the Indian subcontinent. Some of the advantages of this floor system, namely easy construction, technical simplicity and low-cost, made it a popular choice for industrial buildings and URM urban buildings in many countries, as well as for high-rise steel and concrete framed buildings [16].

When steel is used instead of timber, the typical scheme of this flooring system is comprised of steel beam girders and masonry vaults with flat ceramic tiles (in one or two layers) or with hollow bricks. The beams have an I-shaped cross section and can be of a different height, usually between 140 – 240 mm [25]. The spacing between them can be between 600 and 1000 mm. The thickness of the floors can vary from 150 mm up to 200 mm [21]. Generally, the floor beams are supported by the load bearing masonry walls, with a support length of about one-third of the wall thickness. In the ground floors, the

use of steel girders and cast-iron columns results in large open spaces, a typical feature of the buildings in the Eixample district of Barcelona.

The one-way slabs found in the typical Eixample buildings are characterized by beams made of timber, steel or concrete connected with small ceramic barrel vaults. The choice of the material used for the beams depends on the construction period of the building. Timber beams with wood plank pavements were used in the early years of the construction of the Eixample buildings before 1890 [13]. Later and until the middle of the 20th century, the horizontal timber structures described as jack arch floors (*forjados de revoltón* in Spanish) were used as they were popular along the Mediterranean coast of Spain [24].

The introduction of new materials and the industrialization led to the replacement of the timber beams with metallic beam elements as a horizontal structural system [14]. Although steel beams with tile vaults were progressively introduced in the last decade of the 19th century, timber floor systems had been still used in a period of transition that lasted almost 30 years. A metal shortage caused by the Spanish Civil war motivated the use of reinforced concrete beams instead of steel ones [21]. Figure 2 shows the evolution of different solutions for the flooring system across the last 150 years in Catalonia, Spain.

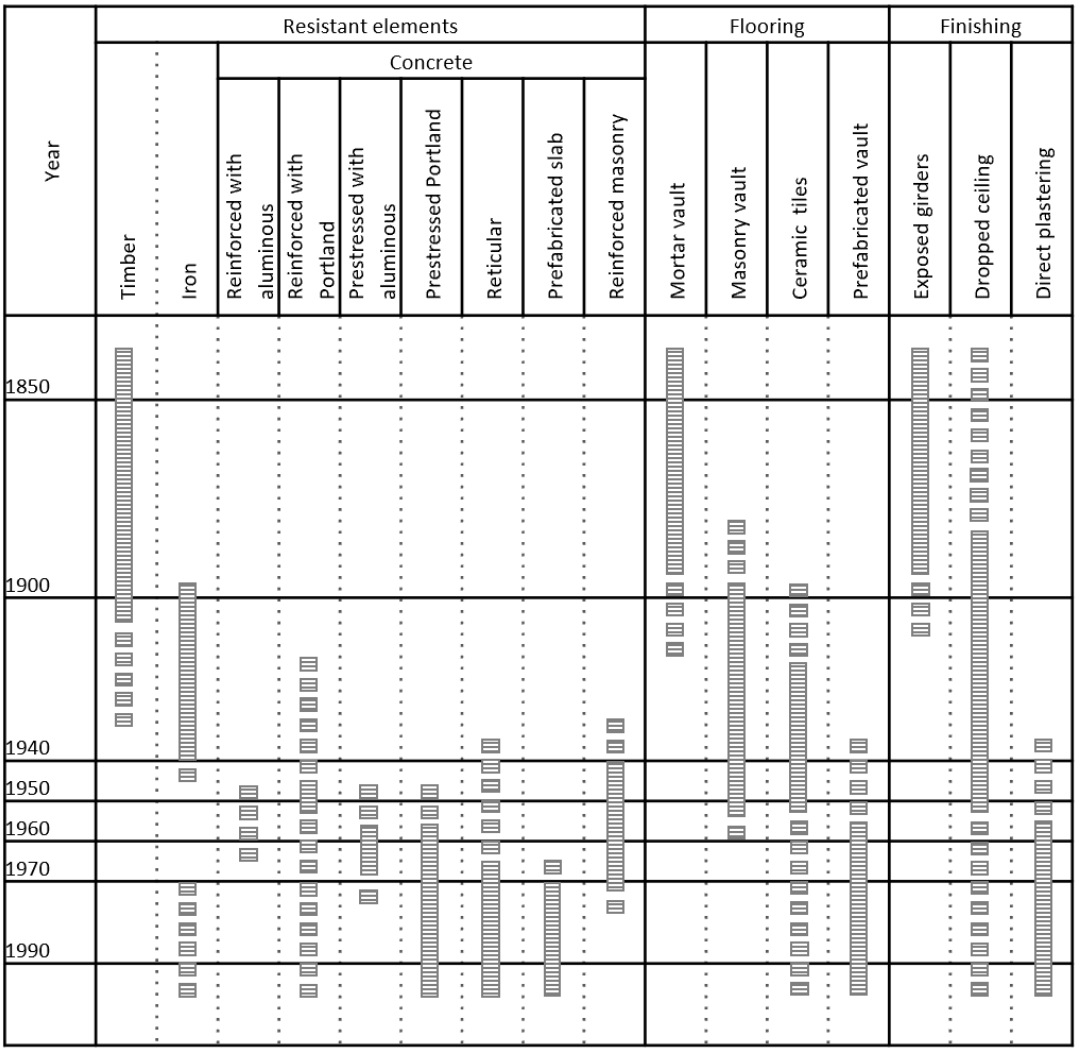

Figure 2 - Use of different types of flooring system in Catalonia since 1850 (Figure adapted from Casanovas et al. [26]).

The one-way floors in the existing buildings of the Eixample district consist of the following elements (Figure 3): 1) one-way timber or steel beams; 2) tile barrel vaults supported by the beams; 3) a layer of rubble or lime mortar used as an infill over the vaults; and 4) an upper layer finished with a pavement on top.

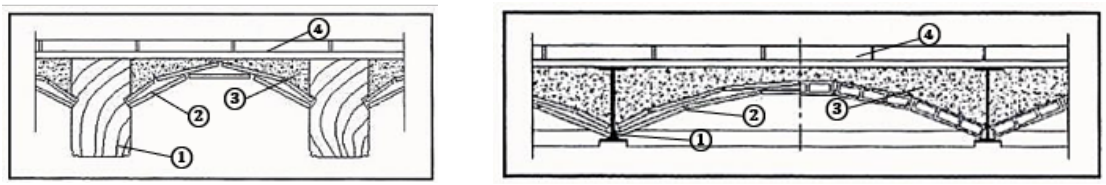

a) b)

Figure 3 - Typical one-way floors in the Eixample district of Barcelona: a) timber beams with tile barrel vaults, and b) steel beams with tile barrel vaults (Figure adapted from Paricio [13]).

The direction of the beams is determined by the geometric plan of the building, and the location of the load bearing walls. In the URM buildings of the Eixample district, the beams of the floors are usually perpendicular to the front and rear façades, and perpendicular to the patios and the staircase boxes (see Figure 4).

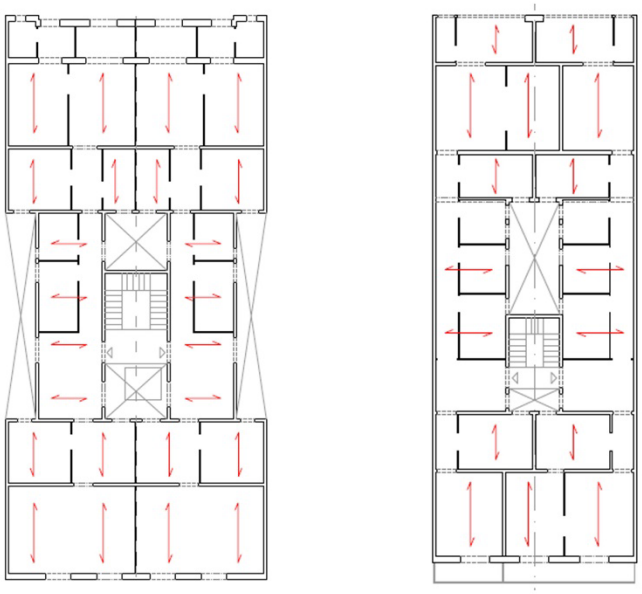

Figure 4 - Floor plan of two typical Eixample buildings illustrating the direction of the floor beams [27].

3. Numerical model of a representative building of the Eixample district of Barcelona

3.1 Geometry and FE mesh

A building taxonomy has been prepared for the purpose of classifying the different structural typologies found in historical building of the Eixample district and to assist the assessment of the seismic vulnerability of representative buildings by means of numerical methods [27,28]. This taxonomy considers parameters that can influence the structural response such as the geometry, material, lateral load bearing system and structural irregularities, among others. Based on this information, the case study considered in this work corresponds to one of the most representative URM building typology in the Eixample district. Figure 5 presents a view of the façade and a floor plan of the selected building. All the information related with the geometry and the structural characteristics is based on the detailed inspection carried out by Cornadó [27].

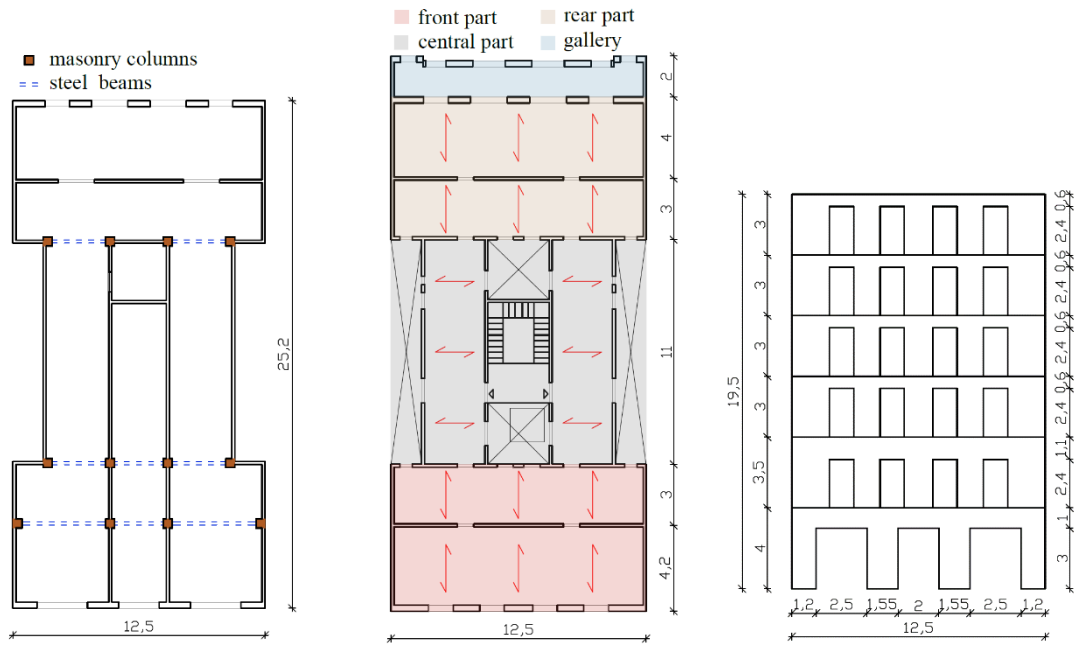

a) b) c)

Figure 5 - Selected representative building of the Eixample district: a) ground floor configuration; b) floor plan section (adapted from Cornadó, 2015 [27]); c) front façade geometry (dimensions in metres).

The URM structure used as a case study was built in 1891 and is located at number 40 of Entença Street in Barcelona. The façade walls have a thickness of 300 mm, while the lateral and interior structural walls have a thickness of 150 mm. Masonry square pilasters of 450 × 450 mm^2 are constructed as part of the lateral walls in order to support the steel truss beams on the ground floor, used to create a large open space for commercial activities (Figure 5a). These steel truss beams are commonly composed of several steel profiles.

The architectural plan of the building has a rectangular shape of 12.50 × 27.15 m^2. The geometrical configuration consists of a central core connecting two symmetrically shaped bays (Figure 5b). The central part consists of an interior patio, a staircase box and two exterior semi-patios. The structure has six storeys, with the first two having different

height compared to the rest of them. The ground floor is 4 m high, the mezzanine floor 3.50 m high and the top four stories are 3.00 m high. The overall height of the building is 19.50 m.

The façade wall presents a well-defined arrangement of four door openings of 1.20 × 2.40 m^2 size at each level except at the front façade of the ground floor, which has three bigger size openings, as this level is used for commercial activities (Figure 5c). The percentage of openings on the façades is notably high, 32.3% at the front façade and 36.2% at the rear façade. Steel beams are used as lintels for all the openings.

The structural behaviour of the building is numerically investigated using continuum Finite Element models. Figure 6 shows a frontal view of the front façade and a generic view of the 3D FEM model, which includes all the structural elements, namely load bearing walls and pillars, steel beams and trusses and floors. The galleries located at the exterior of the rear façade (see Figure 5b) have not been considered as part of the numerical model, as due to their large openings, they are not expected to contribute to the structural performance. Nevertheless, their mass has been applied to the rear façade wall.

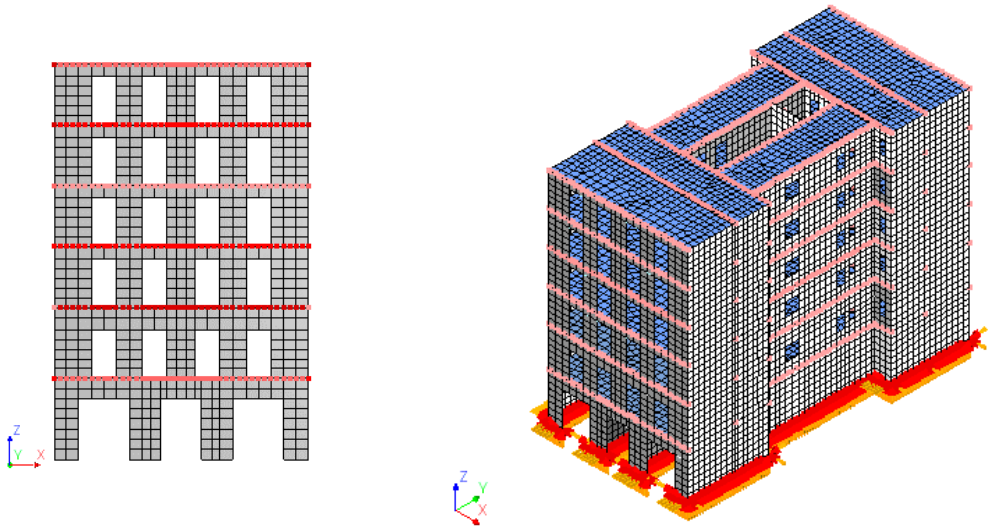

a) b)

Figure 6 - Finite numerical model of a representative building of the Eixample district: a) geometry of the front façade; b) 3D view of the building.

The FEM model has been prepared using the software DIANA-FEA [29]. Quadratic shell elements have been used for modelling the masonry walls and the flexible floors of the building. The used quadratic shell elements (CQ40S) have eight nodes and five degrees of freedom (three translations and two rotations) per each node. The integration scheme is a 3 × 3 Gauss integration over the element's plane, and a Simpson integration scheme with seven points through the thickness of the elements. The 3D beam element CL18B (composed of three nodes and six degrees of freedom for each node) has been used for the modelling of the beams of the ground floor and the lintels above all the openings. The movement of the rotational degree of freedom in Z direction (see Figure 6 for the used axes convention) of the 3D steel elements has been restrained in order to ensure compatibility between beam and shell elements.

The dimensions of the beam elements used in the lintels correspond to steel profiles of IPN240 for the façade openings at the ground floor and IPN140 for the rest of the openings, while the section of the steel profiles at the basement has been manually defined to match the inertia properties of the original steel truss profiles. The FE numerical model is composed of 17,596 shell elements (10,949 shell elements for the URM walls and 6,647 shell elements for the floors), 805 3D beam elements and 3,052 one-node translational mass elements used to provide the loads of the diaphragms. The total number of nodes is 52,155. The final mesh size (with an average element size of 0.5 m), as well as the type of elements and integration scheme, have been selected following a mesh convergence study. The boundary conditions at the base of the building have been assigned as totally fixed by restricting both translational and rotational movements.

The floors have been modelled as one-way diaphragms using quadrilateral (CQ40S) and triangular (CT30S) shell elements. The corresponding permanent and live loads of the floors have been applied only at the walls supporting the floor beams. The longitudinal axis of the floor beams is orthogonal to the façade walls for the floors located in the front and rear bays, and it is parallel to the façade for the beams of the floors located in the central part (Figure 5b). The roof has the same one-way slab construction of the floors, which provides regularity to the structure, and has facilitated the addition of storeys at the top in many buildings in Eixample. In this work, wall-to-floor connections are assumed as fixed, as focus is given in the evaluation of the effect of the in-plane stiffness of the one-way floors. Therefore, any local failures due to sliding between the floor beams and walls are not considered.

The loads acting on the structure have been defined according to the provisions of the Spanish norm [30] and are shown in Table 1. The dead load of the floor diaphragms includes the weight of the beams (steel or timber), the rubble infill and the pavement. In addition to the live load of 2 kN/m^2, a load of 1 kN/m^2 has been added to the floors, corresponding to the division walls and the potential addition of new pavements, which is common in Eixample buildings following past rehabilitation works. The weight considered during the seismic event has been defined according to NRE-AEOR-93 [25] as the entire self-weight load and 30% of the live load applied to the typical one-way floors. As already mentioned, in order to simulate correctly the loading conditions given by the one-way floor systems, the load of the floors was applied as a concentrated mass to the nodes at the edge where the beams of each floor are connected with the lateral walls.

Table 1 - Loads used in the numerical models of the representative building

Load	[kN/m^2]
Floor structural system (steel beams and masonry vaults)	2.45
Floor structural system (timber beams and masonry vaults)	1.25
Pavement	1
Division walls	1
Live load	2

3.2 Material properties of the representative building

Masonry is simulated as a continuum material with properties corresponding to the average response of the composite material. Its nonlinear behaviour is considered through the

use of the Total Strain Fixed Crack model implemented in DIANA-FEA software [29]. This constitutive model has been commonly used in the literature to simulate the nonlinear response of unreinforced masonry [31–34]. A parabolic softening curve has been used under compression and an exponential softening curve under tension. The shear behaviour after cracking has been described through a constant shear stiffness reduction with a shear retention factor of 0.01. Table 2 presents the mechanical properties used for the URM walls in all the simulations.

Table 2 - Material properties of the unreinforced masonry walls in the numerical models

Masonry walls			**Reference**
Young's modulus	1800	MPa	[35]
Poisson's ratio	0.2	[-]	[36]
Mass density	1800	kg/m^3	[36]
Compressive strength	4.0	MPa	[35,36]
Compressive fracture energy	6400	N/m	[37]
Tensile strength	0.08	MPa	Defined
Tensile fracture energy	50	N/m	[28]

Different values ranging between 1.8 MPa and 4.0 MPa have been reported by previous studies for the compressive strength of the masonry walls in existing buildings located in the Eixample district of Barcelona [20,21,25]. This work considers the values for the Young's modulus and the compressive strength derived from the experimental tests done at the Polytechnic University of Catalonia (UPC) on specimens extracted from existing buildings in Barcelona [35]. These values correspond to the upper bound of the values given by the Italian Code for solid brick masonry [36]. The value of the mass density has

been selected according to the recommendations of the Italian code for solid brick masonry [36].

The tensile strength corresponds to 2% of the compressive strength. This value is lower than the one given as a function of the shear strength as $ft=1.5\tau_0$ [38] considering a shear strength of $\tau_0=0.12\ MPa$ according to Moreno-González [39]. The lowest between these two values has been chosen as being more representative of the low properties of the mortar used in the Eixample buildings.

The value of the compressive fracture energy has been defined as a function of the compressive strength according to Lourenço [37]:

$$G_f^c = df_c \quad (1)$$

where d =1.6 mm. For the tensile fracture energy, a value of 50 N/m has been used as in previous studies of the representative buildings in Dimovska et al. [28].

The mechanical properties for the steel beams have been defined according to Moreno-González and Bairán [39], and have been used for the steel beams in the ground floor, as well as for the lintels in the numerical models of the representative buildings (Table 3).

Table 3 - Material properties of all the steel beams in the numerical models

Steel beams			**Reference**
Young's modulus	210000	MPa	[39]
Poisson's ratio	0.3	[-]	[39]
Mass density	7850	kg/m^3	[39]

The one-way floors have been simulated as an orthotropic elastic material. The elastic properties are presented in Table 4 and Table 5 for steel and timber beam one-way floors,

respectively. The procedure for the derivation of these orthotropic elastic properties of one-way floors is the core of this work and is presented in the following section.

Table 4 - Material properties of the one-way diaphragm with steel beams and masonry vaults

Elastic properties		
E_x	1000	MPa
E_y	7800	MPa
$G_{xy\perp}$ (perpendicular to the beams)	27	MPa
$G_{xy\parallel}$ (parallel to the beams)	110	MPa
ν_{xy}	0.06	[-]

Table 5 - Material properties of the one-way diaphragm with timber beams and masonry vaults

Elastic properties		
E_x	1100	MPa
E_y	4000	MPa
$G_{xy\perp}$ (perpendicular to the beams)	27	MPa
$G_{xy\parallel}$ (parallel to the beams)	46	MPa
ν_{xy}	0.10	[-]

4. Finite element modelling of the jack arch floors

4.1 Geometry and FE mesh

This section presents the *detailed 3D solid* and the *simplified 2D shell* finite element models that are used to evaluate the in-plane stiffness of one-way jack arch floors. Figure 7 and Figure 8 illustrate two typical floors that can be found in the Eixample buildings. The vaults in both cases are made of thin clay tiles and a compression layer of rubble material. Different materials are used for the one-way beams, namely steel and timber.

The geometry of the jack arch floors has been defined according to previous research studies related with the structural elements in the representative building typologies of Eixample [13]. This information was supported by reports of rehabilitation works carried out on existing buildings, and by original design plans of buildings found in the public archive of Barcelona.

The first model consists of steel beams spaced at a distance of 700 mm and the second model has timber beams spaced at a distance of 550 mm. In both cases, the vaults are composed of a double layer of thin clay tiles, and the compression layer on top of them is a rubble material. Figure 7 and Figure 8 present the geometrical characteristics of the steel and timber jack floors, respectively.

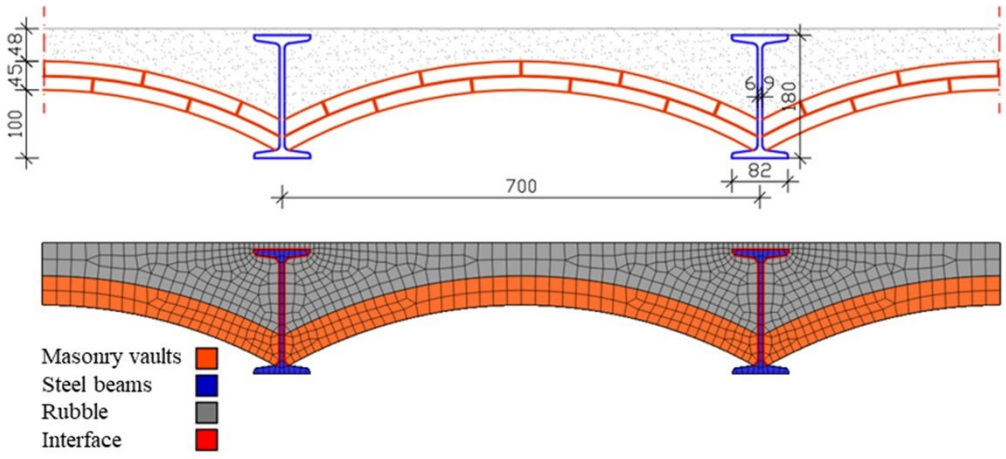

Figure 7 - Section of the jack arch floor with steel beams and tile barrel vaults: Geometry (top) and finite element model (bottom) (dimensions in mm).

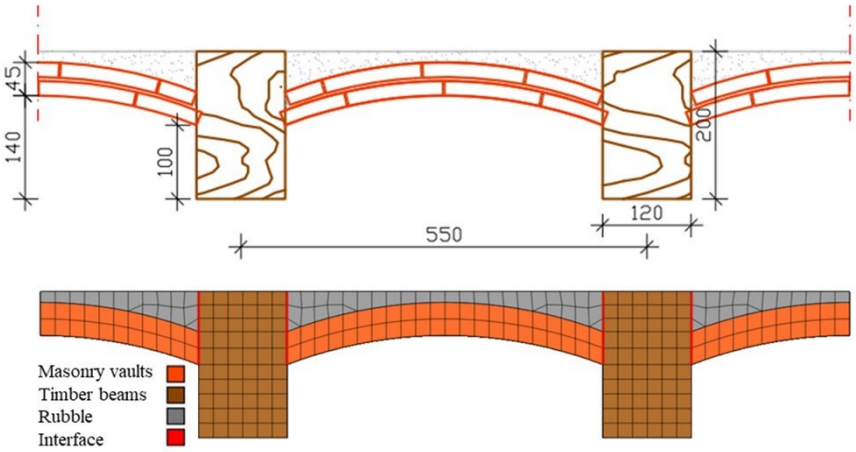

Figure 8 - Section of the jack arch floor with timber beams and tile barrel vaults: Geometry (top) and finite element model (bottom) (dimensions in mm).

The 3D finite element models of the two floors (referred hereafter as *3D solid floor model*) have been prepared using DIANA-FEA software [29]. The models consider a full vault and two halves at each side with overall dimensions 1.40 m × 4.00 m for the floor with steel beams, and 1.10 m × 4.00 m for the floor with timber beams (see Figure 9). The length of the floor models is assumed to be 4.00 m as this is the most typical dimension for the one-way floors of Eixample buildings. The finite element meshes consist of eight-node (HX24L) and six-node (TP18L) solid brick elements, based on linear interpolation and standard Gauss integration. Interface elements (Q24IF) have been used to define the interface between the beams and the vaults and between the rubble material and the beams.

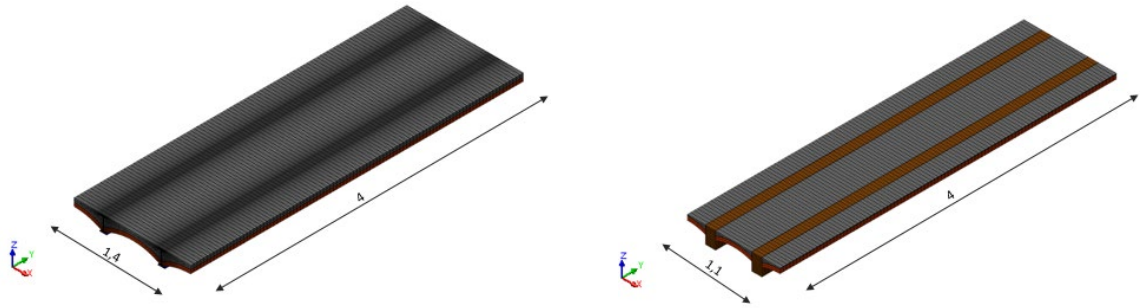

a) b)

Figure 9 - 3D solid finite element models of the floor system with tile vaults and: a) steel beams; b) timber beams (dimensions in metres).

The simplified 2D shell models (referred hereafter as *2D shell floor model*) follow the same modelling approach used for the simulation of the floors in the models of the whole buildings (see Section 3.1). The 2D shell floor model is made of the quadratic shell elements (CQ40S) by considering an orthotropic elastic behaviour.

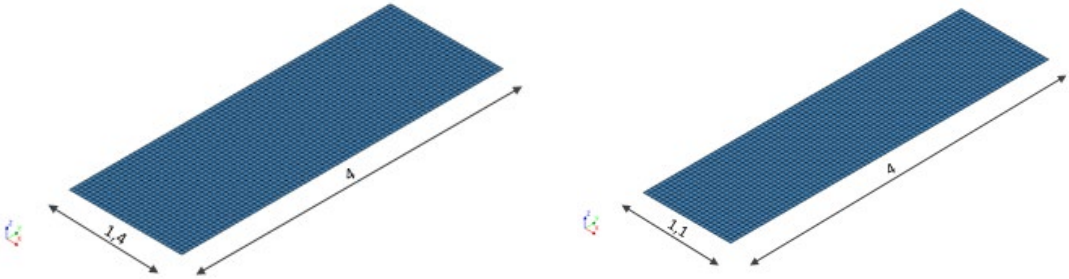

a) b)

Figure 10 - 2D equivalent shell model: a) floor model with steel beams; b) floor model with timber beams (dimensions in metres).

The 2D shell models for the two floors have the same length, width and volume with their corresponding 3D solid models (Figure 10). Their thickness is constant and defined such that the sections orthogonal to the longitudinal axis of the beams are equal in terms of area to those of the detailed 3D models. This results to an equivalent thickness of 121.4 mm for the floor with steel beams and 100.8 mm for the floor with timber beams.

4.2 Material properties for the 3D solid FE floor models

Similar to the masonry walls of the 3D building models, the mechanical behaviour of both masonry and the rubble material has been simulated with the Total Strain Fixed Cracking model of the DIANA-FEA software [29]. The tensile response has been characterized by a linear behaviour up to the tensile strength followed by an exponential softening. The compressive response has been represented by a parabolic hardening and softening. The shear behaviour has been assumed as constant with a shear retention factor of 0.01. In both cases, the stress-strain curves have been regularized considering the fracture energy and the characteristic length of the material. A linear elastic behaviour has been adopted for the steel and timber elements. This modelling approach has been used successfully in the past for simulating masonry vaults with steel elements in historical buildings of Barcelona [40].

Table 6 - Material properties of the ceramic tile vaults, rubble, steel beams with corresponding interface elements, and timber beams with corresponding interface elements in the 3D solid numerical models of the jack arch floors

Material properties			Reference
Masonry vaults			
Young's modulus	1800	MPa	[35]
Poisson's ratio	0.2	[-]	[36]
Mass density	1800	kg/m^3	[36]
Compressive strength	4.0	MPa	[35,36]
Compressive fracture energy	6400	N/m	[37]
Tensile strength	0.08	MPa	Defined
Tensile fracture energy	50	N/m	[28]
Rubble			
Young's modulus	690	MPa	[41]
Poisson's ratio	0.2	[-]	[36]
Mass density	1900	kg/m^3	[36]
Compressive strength	1.0	MPa	[41]
Compressive fracture energy	1600	N/m	[37]
Tensile strength	0.02	MPa	Defined
Tensile fracture energy	20	N/m	Defined
Steel beams			
Young's modulus	210000	MPa	[39]
Poisson's ratio	0.3	[-]	[39]
Mass density	7850	kg/m^3	[39]
Interface elements between steel and masonry			
Normal Stiffness	200	N/mm^3	[40,42]
Shear stiffness	100	N/mm^3	[40,42]
Cohesion	0.1	MPa	[43]
Frictional angle	26.5	°	[44]
Timber beams			
Young's modulus	8000	MPa	[30]
Poisson's ratio	0.3	[-]	[45]
Mass density	520	kg/m^3	[45]
Interface elements between timber and masonry			

Normal Stiffness	200	N/mm^3	[40,42]
Shear stiffness	100	N/mm^3	[40,42]
Cohesion	0.1	MPa	Defined
Frictional angle	30.96	°	[46]

Table 6 presents the material properties used in the 3D solid models of the typical jack arch floors. The masonry vaults have been modelled with the same material properties as the masonry walls in the numerical model of the representative building (see Section 3.2). The properties of the rubble material have been defined according to the experimental results in Segura et al. [41] and the selected values are also in line with the lower bound for rubble masonry in the Italian guidelines [36]. The value for the compressive fracture energy has been obtained following the recommendations from Lourenço [37], as explained in the Section 3.2. A value of 20 N/m has been defined for the tensile fracture energy.

The mechanical properties for the steel beams are the same as the ones used for the steel lintels as presented in Table 6. A Coulomb friction model has been used for the simulation of the interface between beams and bricks and rubble. The values for the normal and shear stiffness have been defined according to Endo et al. [40,42]. Since the information in the literature regarding the frictional behaviour between steel and masonry or rubble materials is very limited, the frictional parameters have been considered conservatively equal to the ones used in the literature for describing a contact surface between steel and concrete. A value of 0.1 MPa has been chosen for the cohesion as used in Campione et al. [43] for the simulation of frictional effects in structural behaviour of no-end-connected steel-jacketed reinforced concrete columns. This value corresponds to an upper

bound value for an interface between concrete and steel according to Adam et al. [47] The frictional angle is 26.5º (tanϕ = 0.5), corresponding to a value for an interface between steel and concrete according to PCI Industry Handbook Committee [44].

The last part of Table 6 presents the material properties for the timber and the interface elements used in the 3D solid model of the one-way flexible floor with timber beams and masonry vaults. In most of the buildings with timber floors in the Eixample district, the timber beams are made out of Pine wood (Pinus sylvestris), which can be easily found in the Pyrenees [13]. The Young's modulus of this type of timber is defined as equal to one of the lower resistance class C16 in the Spanish code for construction with timber [30]. The density and Poisson's coefficient have been chosen according to the physical properties of Pine wood [45]. Due to the lack of information for the cohesive properties between timber and masonry materials, the properties of the interface elements are conservatively chosen the same as in the floor model with steel beams. The value for the frictional angle has been obtained according to a static frictional coefficient tanϕ=0.6 (frictional angle of 30.96º) between timber and brick [46].

5. Numerical analyses of the jack arch floor systems with steel and timber beams

The aim of the numerical analyses of this section is the estimation of the orthotropic elastic properties of the two types of jack arch floors that are necessary for their simplified modelling using shell elements in FEM models of URM buildings, as discussed in Section 3.1. As described previously (Section 4.1), a detailed 3D solid FE model (called 3D solid floor model) has been prepared for computing the elastic orthotropic properties of the

jack arch floor systems and use them in a simplified 2D shell FE model (called 2D shell model). It has not been possible to validate the numerical analyses by comparison with experiments, because experimental data at structural level on the floor slab system have not been so far carried out. Therefore, numerical simulations are used as a virtual laboratory to obtain the desired orthotropic properties of the floors. In the following sections, the necessary parameters for the definition of the orthotropic elastic behaviour are computed, namely three Young's moduli, three shear moduli and three Poisson's coefficients.

5.1 Evaluation of the Poisson's coefficients

The Poisson's coefficients of the 3D solid floor model have been computed by performing three linear elastic analyses. In particular, for each of these analyses a compressive distributed load is applied at one of the faces (Figure 11) and the ratio between transversal and axial deformation has been computed, as shown in equations (2) – (4) .

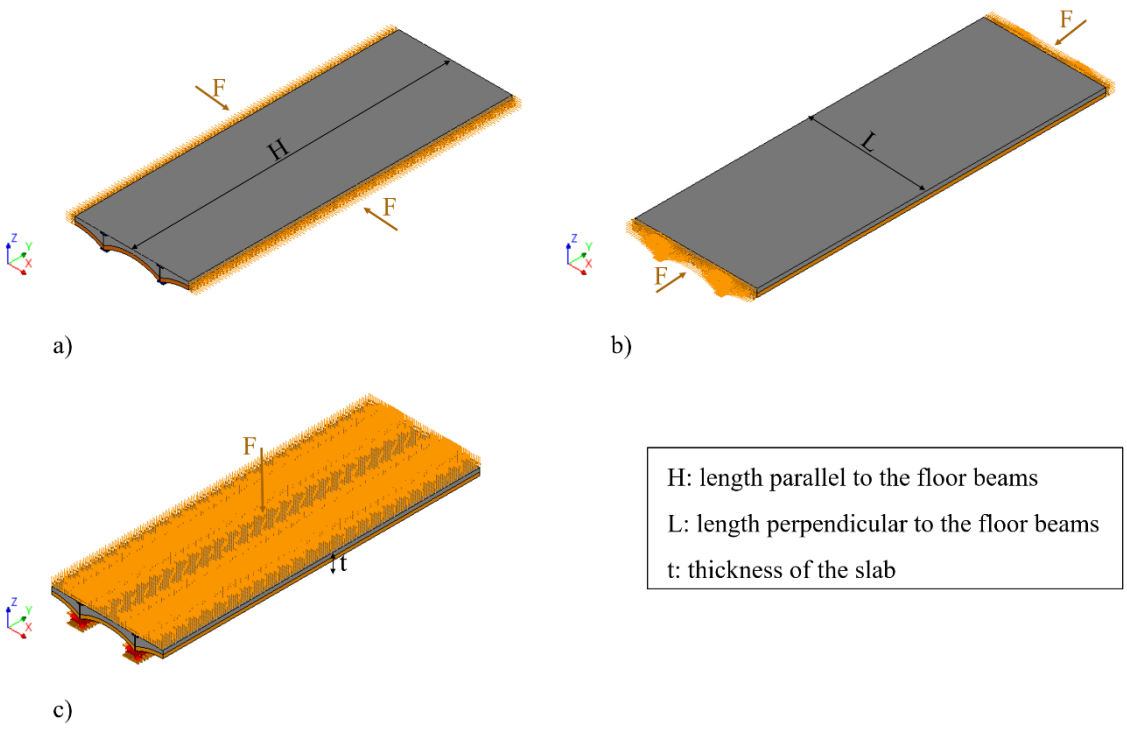

Figure 11 - Loading conditions for 3D solid floor model in order to obtain: a) Poisson's coefficients v_{xi} with i =y;z; b) Poisson's coefficients v_{yi} with i =x;z; c) Poisson's coefficients v_{zi} with i =y;x

$$\varepsilon_x = \frac{\Delta L}{L} \tag{2}$$

$$\varepsilon_y = \frac{\Delta H}{H} \tag{3}$$

$$\varepsilon_z = \frac{\Delta t}{t} \tag{4}$$

In the above equations, ΔL, ΔH and Δt correspond to the average change in the width (L), length (H) and thickness (t) of the floor, after the application of the load.

The following equations (5) - (7) have been used to estimate the Poisson's coefficients (v_{xy}, v_{yz} and v_{xz}), which are required for the elastic orthotropic material in DIANA-FEA

software [29]. The other three Poisson´s coefficients are calculated considering the symmetry of the orthotropic stiffness matrix, as follows:

$$\nu_{xy} = -\frac{\varepsilon_y}{\varepsilon_x} \tag{5}$$

$$\nu_{yz} = -\frac{\varepsilon_z}{\varepsilon_y} \tag{6}$$

$$\nu_{xz} = -\frac{\varepsilon_z}{\varepsilon_x} \tag{7}$$

Table 7 - Values for the Poisson's coefficients used in the 2D shell floor models

Poisson's coefficients	**Floor system with steel beams**	**Floor system with timber beams**
ν_{xy}	0.06	0.10
ν_{yz}	0.14	0.17
ν_{xz}	0.23	0.20

Table 7 presents the computed values of the Poisson's coefficients, which are used later in the numerical model of the representative Eixample buildings. The computed values satisfy the conditions (8) and (9) for an orthotropic material [29,48]:

$$\nu_{xy}^2 < \frac{E_x}{E_y}, \nu_{yz}^2 < \frac{E_y}{E_z}, \nu_{xz}^2 < \frac{E_x}{E_z} \tag{8}$$

$$2\nu_{xy}\nu_{yz}\nu_{xz}\frac{E_z}{E_x} < 1 - \nu_{xy}^2\frac{E_y}{E_x} - \nu_{yz}^2\frac{E_z}{E_y} - \nu_{xz}^2\frac{E_z}{E_x} \leq 1 \tag{9}$$

5.2 Evaluation of the Young's and shear moduli

5.2.1 FEM analyses of the 3D solid and 2D shell floor models

The evaluation of the Young's and shear moduli of the orthotropic material used to simulate the floors in the building model has been made through the direct comparison of the in-plane response under uniaxial and shear loading of the 3D solid model of the floors and 2D shell model of each floor type with elastic orthotropic properties. The same loading conditions have been applied to both 3D solid and 2D shell floor slab models in order to allow the estimation of their axial and shear stiffness.

First, the values of the Young's moduli for the elastic orthotropic material of the 2D shell models have been computed along the local in-plane axes X and Y by matching the elastic axial stiffness of the 3D solid floor models. Accordingly, a set of two analyses per floor type have been carried out with the 3D solid floor models in order to evaluate the axial stiffness of the two floors by applying a compressive load along the two axes of orthotropy, i.e parallel and orthogonal to the beams. Figure 12 presents the force-displacement curves obtained from these analyses for the two floor systems. For load applied perpendicular to the beams, the capacity curves present a first linear range followed by a hardening branch. This behaviour is observed for the slabs with either steel or timber beams. For loading parallel to the beams, the force-displacement curves present a linear elastic behaviour up to a displacement of 3 mm. The differences between the two analyses reveal the orthotropic behaviour of the floor. As expected, the stiffness is higher for a loading parallel to the longitudinal axis of the floor beams, due to the higher contribution of the beam stiffness to the total stiffness of the floors. On the contrary, the lower stiffness

of the floor in a direction perpendicular to the longitudinal axis of the beams results in a higher deformation of the masonry vaults and subsequently their damage. This drop in the global stiffness due to the damage in the vaults is illustrated by the nonlinear force displacement response shown in Figure 12 (left).

The initial values for the Young's moduli in the two directions of orthotropy have been chosen such that the axial stiffness of the 2D shell models is equal to the initial (elastic) axial stiffness of the 3D solid floor models, see Table 10.

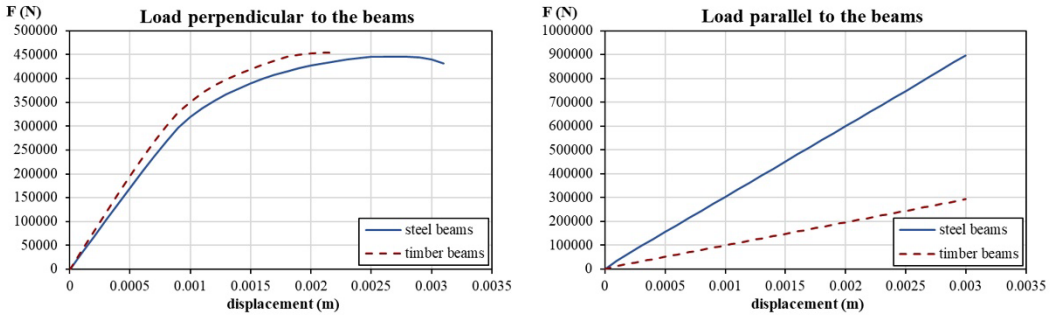

Figure 12 - Load-displacement curves derived from a compression test of the 3D solid floor models in X direction (perpendicular to the beams, left) and in Y direction (parallel to the beams, right).

Once the elastic modulus has been calibrated, a simple shear configuration has been used for the estimation of the shear modulus by considering the same boundary conditions that these one-way floors have in the existing building. This configuration has been previously verified by means of a simple elastic analysis comparing the states of simple shear and pure shear. The shear modulus G_{xy} of the 2D shell models has been computed by matching the elastic shear stiffness of the 3D solid floor models. Thus, two analyses have been performed using the 3D solid model for each floor system inducing a shear defor-

mation of the floor, by applying a horizontal displacement at one end of the floor (restraining the vertical displacement) and keeping the opposite end fixed. The displacement is orthogonal to the longitudinal axis of the beams in the first analysis, in order to obtain the shear modulus of a floor with beams orthogonal to the seismic load ($G_{xy\perp}$), and parallel to them in the second one for obtaining the shear modulus of a floor with beams parallel to the loading direction ($G_{xy\parallel}$). It is worth noticing that the parameters $G_{xy\perp}$ and $G_{xy\parallel}$ have been artificially introduced to distinguish the two different loading procedures assumed to evaluate the shear modulus G_{xy}. Figure 13 and Figure 14 present the contour of the horizontal displacements of the floor for a loading of 0.5 mm in the X direction (orthogonal to the beams) and in the Y direction (parallel to the beams), respectively. Figure 15 shows the force-displacement capacity curves obtained from the in-plane shear analyses of these 3D solid floor models for the two loading directions. The capacity curves, obtained from the loading applied perpendicular to the beams, present a similar nonlinear behaviour for both types of floor. For this loading direction, the floor with steel beams is stiffer and shows higher capacity than the one with timber beams. The first branch of the curves obtained for loading parallel to the beams is similar for the two types of floor slabs investigated. However, the floor slab with timber beams reaches a lower ultimate strength than the one with steel beams for the investigated levels of displacements. In both cases, the nonlinear response is due to shear cracking at the masonry vaults and sliding at the masonry-beam interface.

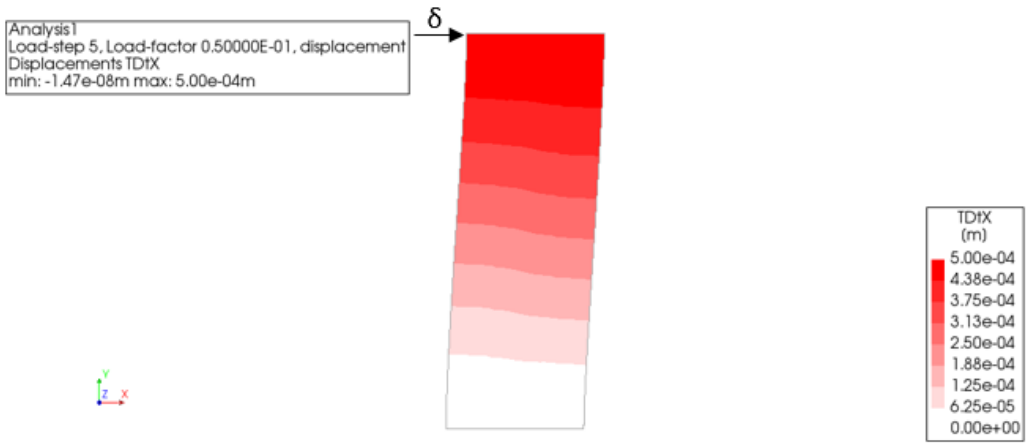

Figure 13 - Displacements in X direction of the 3D solid floor model with steel beams from a displacement load of 0.5 mm applied orthogonal to the beams.

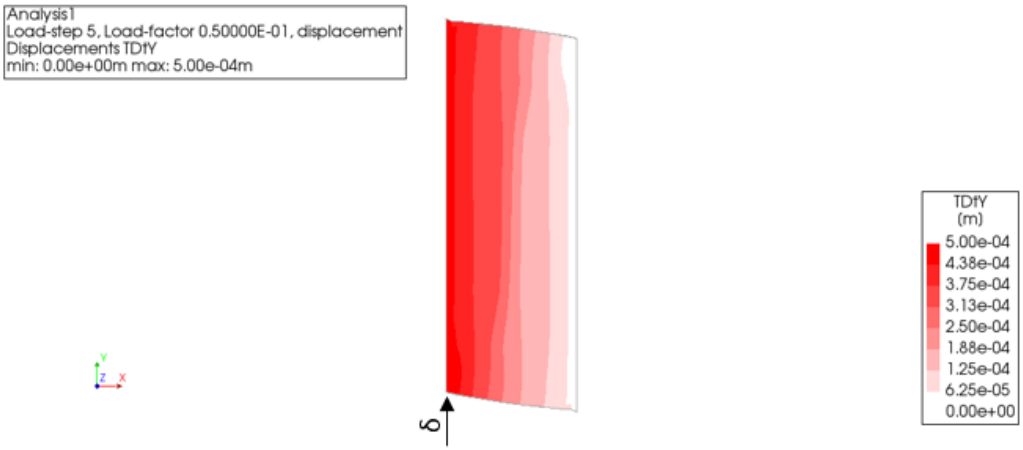

Figure 14 - Displacements in Y direction of the 3D solid floor model with steel beams from displacement load of 0.5 mm applied parallel to the beams.

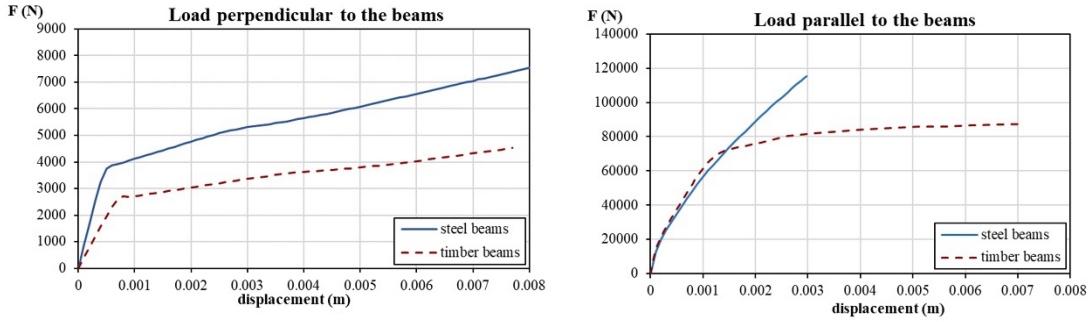

Figure 15 - Load-displacement capacity curves obtained from in-plane shear tests of the 3D solid floor models in X direction (perpendicular to the beams, left) and in Y direction (parallel to the beams, right).

Similar to the case of the Young's moduli, the initial assumptions on the values of the G_{xy} of the 2D shell models are such that the shear stiffness of those is equal to the initial (elastic) shear stiffness of the 3D solid floor models (Figure 16 and Figure 17). Table 8 presents the corresponding estimated values for each floor system. These values confirm the orthotropic behaviour of the jack arch floors, in the two principal loading directions (parallel and perpendicular to the beams). The Young's modulus E_z has been assumed equal to the Young's modulus E_y. The shear moduli in the other two planes (G_{yz}, G_{xz}) have been considered equal to G_{xy}.

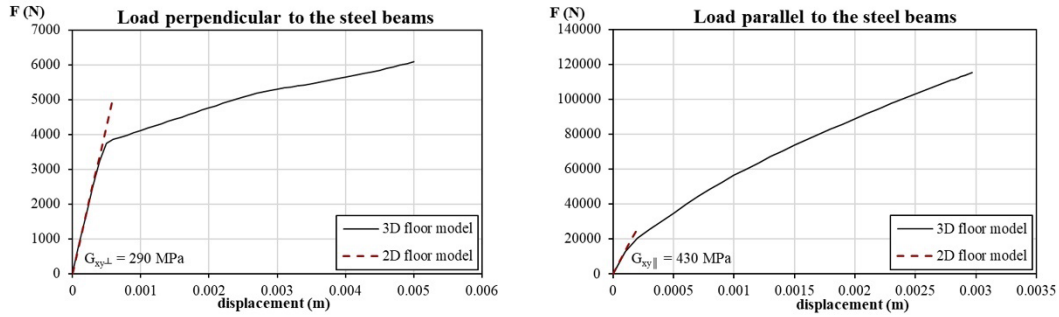

Figure 16 - Calibration of the elastic shear stiffness based on the comparison of the 3D solid and 2D shell floor models with steel beams (for both loading directions).

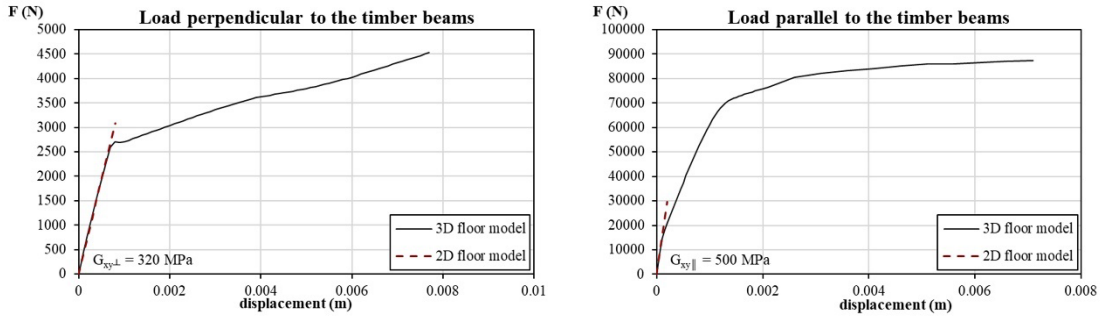

Figure 17 - Calibration of the elastic shear stiffness based on the comparison of the 3D solid and 2D shell floor models with timber beams (for both loading directions)

Table 8 - Values of the elastic properties of the floors obtained from the FEM analyses of isolated floor slab models

Type of floor	**Elastic orthotropic properties**			
	E_x (MPa)	E_y (MPa)	$G_{xy\perp}$ (MPa)	$G_{xy\parallel}$ (MPa)
Floor with steel beams and tile vaults	1000	7800	290	430
Floor with timber beams and tile vaults	1100	4000	320	500

The elastic orthotropic properties obtained from the floor models are different in both floor systems depending on the loading direction. There is a difference of around 65% for the Young's moduli E_y, due to the different material used for the beams in the floor systems and a smaller difference of 10% between the values of the Young's moduli in the direction perpendicular to the beams (E_x), due to the different geometry of the masonry vaults and the material of the beams. The values of the shear moduli $G_{xy\perp}$ and $G_{xy\parallel}$ for the jack arch floor with timber beams are 10% and 16% higher than the ones of the one-way floor system with steel beams.

5.2.2 FEM analyses with a global model of the building

The estimated values of the Young's and shear moduli reported in the previous section were based on FEM nonlinear analyses on isolated detailed 3D solid models of the floor slabs. Such values can be adopted for the simplified 2D shell modelling of the floors under the assumption of elastic behaviour only if the strain/stress admissibility is guaranteed. This check has been performed through a nonlinear seismic analysis of the global FEM model of the selected URM building, including the simplified 2D shell modelling of the floors. The procedure consists in checking if the deformation levels of the 2D shell models of the floor slabs remain in the elastic field during the seismic loading of the entire building, simulated with nonlinear FEM pushover analysis. If the level of deformation experienced by the floors of the building model corresponds to the elastic deformation as identified by the axial and shear tests of the 3D solid floor models (see Section 5.2.1), then the selection of the elastic properties for both models is valid. Contrariwise, if the level of deformation reached by the 2D shell floors in the FEM building model corresponds to a nonlinear behaviour of the 3D solid floor models, then the values of the Young's and shear moduli for the elastic orthotropic material of the floors are updated accordingly (see Figure 18). This updating procedure is iterative, as it will be explained in the following.

The application of the seismic loading to the building models has been simulated through pushover analysis. The analysis includes two steps, the first corresponding to the application of the self-weight and the second to the horizontal loading of the structure

with a force pattern proportional to the distribution of the mass. A Newton-Raphson regular iteration method has been used along with an arc-length for solving the nonlinear system of algebraic equations. The convergence has been checked based on an energy norm by considering a tolerance of 0.001.

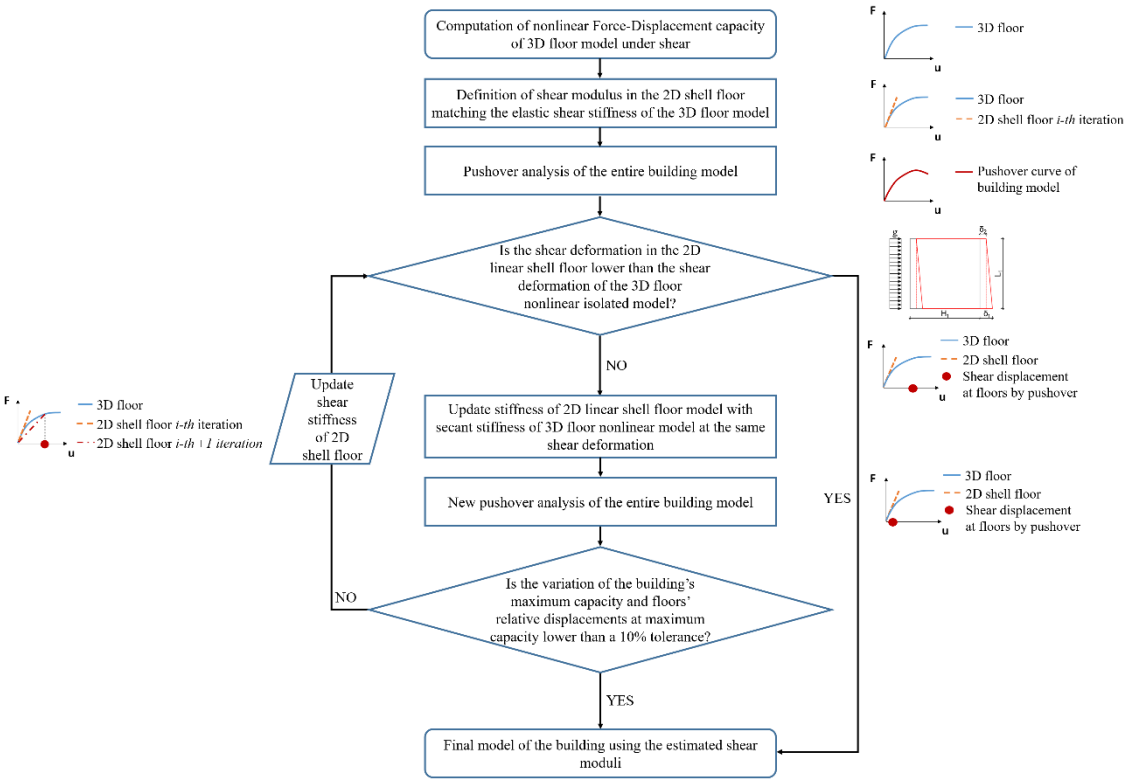

Figure 18 - Flowchart of the numerical procedure used to compute the values of the shear moduli of the jack arch floors.

After performing pushover analyses in X and Y directions, the longitudinal and shear deformations have been computed considering the displacements at the end sides of the top floors of the model. The pushover analysis in X direction provokes a torsional movement of the building (Figure 19a). This is anticipated due to the non-symmetrical distribution of the walls in the front and rear façades, which result in an eccentricity between

the centre of mass and the centre of stiffness of the building. The building is symmetrical in the Y direction and it does not exhibit a torsional response when loaded parallel to it (Figure 19b). Thus, the floor deformations of the building model have been estimated only from the pushover in X direction as this constitutes the only case producing shear deformation to the floors due to the torsional response of the building.

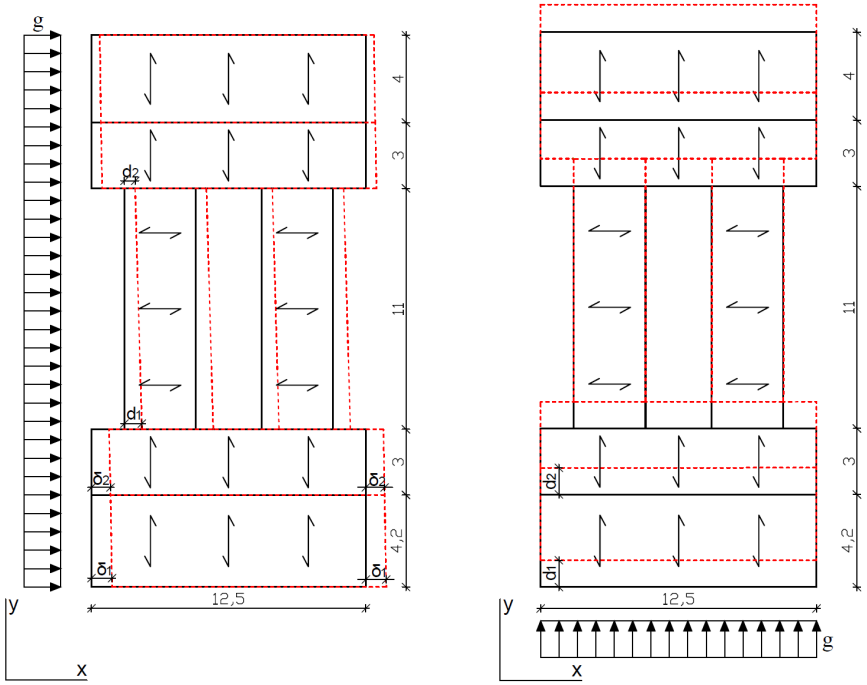

a) b)

Figure 19 - a) Displacements of the floors in the FEM building model from pushover in X direction; b) Displacements of the floors in the building model from pushover in Y direction (dimensions in meters). Red dashed lines illustrate the deformed shape at the maximum load capacity of the pushover analysis (deformation multiplied by 10).

The longitudinal and shear deformations have been used to compare the level of deformations experienced by the 2D shell floors in the global FEM model of the building

with those of the 3D solid models of the isolated floors. The analysis stage used as reference for computing these deformations in the models of the building is the one corresponding to the maximum load capacity. The different levels of the displacements can be visualized in the capacity curves in the Figure 22 for each case. The longitudinal deformation of a floor along the loading direction corresponds to the change in the length of the floor parallel to the loading direction (i.e. its contraction) over the original length (see Figure 20a and Figure 20c). The shear deformation has been computed as the angular distortion of the originally orthogonal floor, see equation (11), as shown in Figure 20b, and Figure 20d. The average values for the displacements of both sides of the floors (marked as ① and ② in Figure 19a) have been considered for the calculation of the longitudinal and shear deformation, as they present the maximum deformation during the performed analyses.

With reference to Figure 20a and Figure 20b, longitudinal and shear deformations of the floors in the models of the building from the pushover in X direction have been computed using the equations (10) and (11).

$$\Delta u = \frac{u_1 - u_2}{H_1} \tag{10}$$

$$\theta = \frac{\delta_1 - \delta_2}{L_1} \tag{11}$$

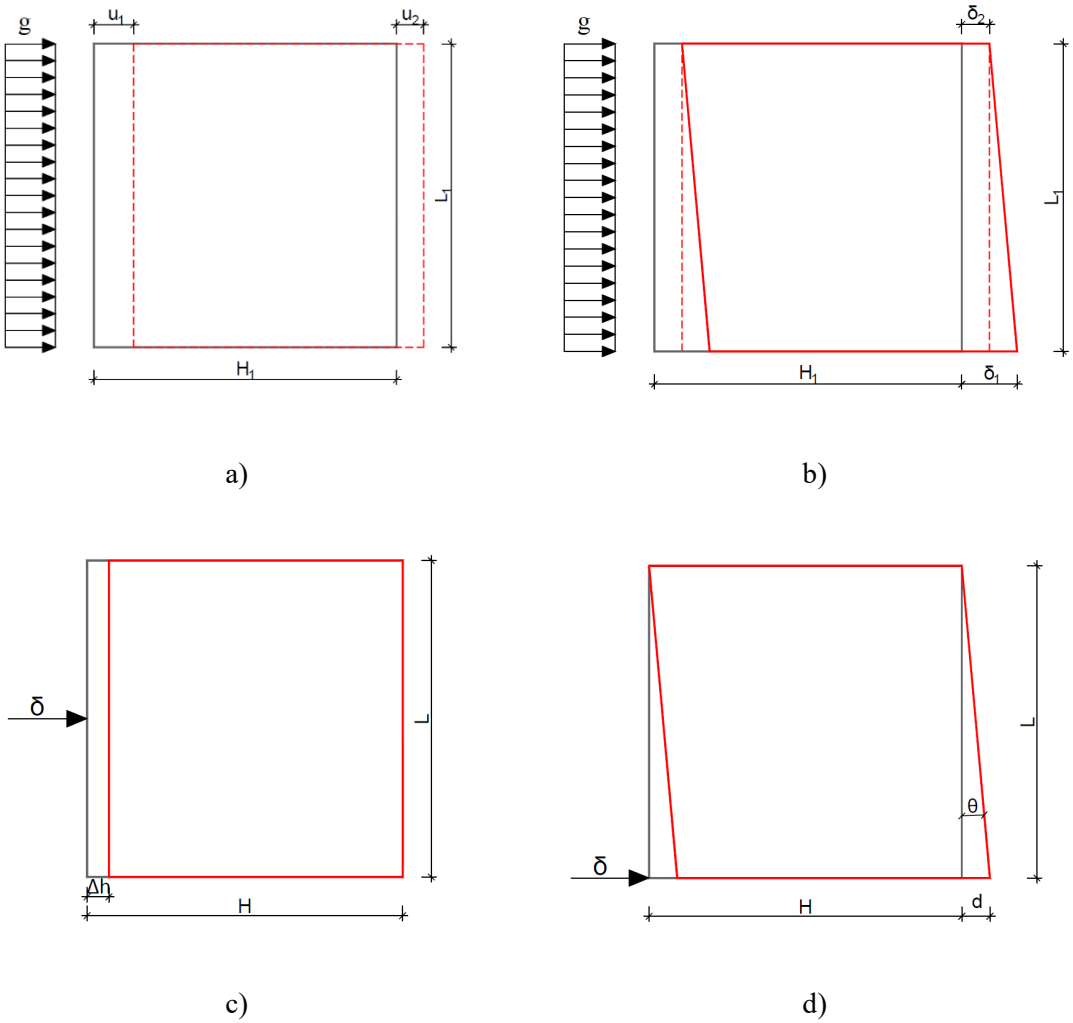

Figure 20 - Longitudinal and shear deformation modes: a) longitudinal deformation in X direction of the floors in the FEM building model; b) shear deformation of the floors in the FEM building model; c) longitudinal deformation in X direction of the 3D solid floor model; d) shear deformation of the 3D solid floor model.

These deformations have been compared to the ones of the 3D solid models of the floors, which have been computed using the equations (12) and (13), see Figure 20c and Figure 20d. The relative displacements from the floors with maximum deformation of the building model have been calculated according to the equations (14) and (15).

$$\Delta u = \frac{\Delta \mathrm{h}}{H} \tag{12}$$

$$\theta = \frac{d}{L} \tag{13}$$

$$\Delta \mathrm{h} = \left(\frac{u_1 - u_2}{H_1}\right) \cdot H\ [m] \tag{14}$$

$$d = \left(\frac{\delta_1 - \delta_2}{L_1}\right) \cdot L\ [m] \tag{15}$$

With regard to the longitudinal deformations, the values computed for all the floor types and for both pushover directions fall within the linear range of the capacity curves of the 3D solid floor slab model. Therefore, the Young's moduli in both directions of the floor systems have been considered equal to the values shown in Table 8.

Contrary to the longitudinal deformations, the shear ones experienced by the 2D shell floors of the building models fall beyond the elastic range of shear deformations as computed by the 3D solid floor slab models. This implies that the floors in the FEM model of the building present an excessive in-plane shear stiffness that should be reduced in order to satisfy the shear-strain admissibility derived from the previous nonlinear analyses of the 3D solid floor models. Hence, the shear modulus computed for the 2D shell floor models has been reduced and an "effective" shear stiffness has been adopted instead of the elastic one of the 3D solid floor models.

The steps to compute the new values of this effective floor stiffness are the following: i) computation of the equivalent shear deformation of the 3D solid floor slab model corresponding to the shear deformation calculated in the 2D shell floors of the building model; ii) computation of the secant stiffness of the 3D solid floor model corresponding

to the computed shear deformations of the 2D shell floors of the building model; iii) update of the shear modulus of the 2D shell model so that its effective shear stiffness matches the secant stiffness computed for the nonlinear 3D solid floor model; iv) execution of a new pushover analysis and computation of shear deformation at maximum capacity. After the execution of the new pushover analysis, a check has been carried out considering two factors (Table 9 and Table 10): i) change of maximum capacity from the pushover analysis in X direction, and ii) change of relative displacements (δ_1-δ_2) in the floors (with beams parallel and perpendicular to the loading direction) corresponding to the maximum capacity of the building model. The iterative procedure has been finalized when the changes are below 10% (based on previous experience) between two successive iterations. Figure 18 shows a visual summary of the entire procedure.

The iterative procedure has been followed only for loading in the X direction, which, as it is already mentioned, is the case producing shear deformation to the floors due to the torsional response of the building. At each iteration, the deformation levels have been checked and the shear moduli have been updated, if necessary, for both floors with beams parallel and orthogonal to the loading direction.

Figure 21a and Figure 21b show the effective stiffness values of the 2D shell floor models obtained from the procedure for the floors with steel beams parallel and orthogonal to the loading direction, respectively. Convergence of the two monitored parameters, i.e. maximum force capacity and local relative displacements of the floors, was achieved after four iterations.

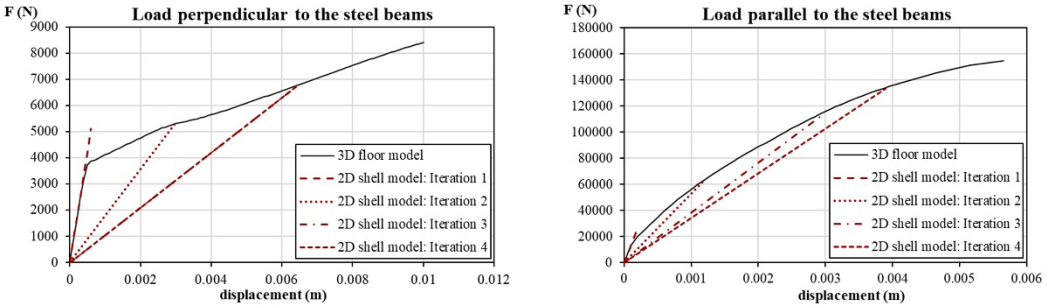

a) b)

Figure 21 - Calibration of the effective shear stiffness of the 2D shell model in the 3D building model: a) floors with steel beams parallel to the loading direction; b) floors with steel beams perpendicular to the loading direction.

Figure 22 presents the capacity curves of the building with steel and timber beam floors for the different iterations. These pushover (acceleration-displacement) curves in X direction indicate differences in both capacity and ductility of the building model after modifying the elastic properties of the floors at each iteration. The building model with elastic properties of the 2D shell floors equal to those of the 3D solid model (first iteration) has the highest maximum capacity and lowest ductility. There is a drop of 8% for the maximum capacity of the building model after the second iteration. On the contrary, the ductility of the building increases with the change of the elastic properties in the 2D shell floors obtained by assuming the secant stiffness of the 3D solid floor model corresponding to the computed shear deformations of the floors of the building model. This result confirms the important influence of the in-plane stiffness of the one-way floors in the global behaviour of the URM building.

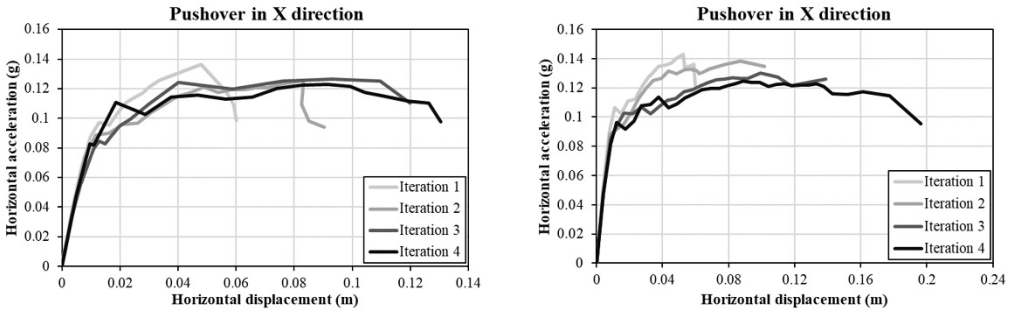

Figure 22 - Capacity curves from pushover analyses in X direction with different shear moduli for the one-way flexible floors: a) floors with steel beams; b) floors with timber beams.

Table 9 summarizes the values of the monitored parameters during the iterative procedure. The difference in the values of the shear moduli between the first iteration and the second one is around 143% in the floor with beams aligned with the X direction ($G_{xy\parallel}$), and around 87% in the floor with beams aligned with Y direction ($G_{xy\perp}$). The same difference between the second and the third iteration is smaller, around 56% for $G_{xy\perp}$ and 34% for $G_{xy\parallel}$. Lastly, the values of the shear moduli of the fourth iteration have converged, with an identical value for $G_{xy\perp}$ and around 9% difference for $G_{xy\parallel}$. The differences in the control values of the maximum capacity and relative displacement of the floors with beams perpendicular to the loading direction are 2.4% and 6%, respectively. The converged values of $G_{xy\perp}$ and $G_{xy\parallel}$ are 9.3% and 25.6% of the elastic ones considered in the first iteration.

Table 9 - Values obtained of the shear properties of the floor system with steel beams after the proposed iterative procedure

Convergence of the shear properties for the floors with steel beams				
Properties	Iteration 1	Iteration 2	Iteration 3	Iteration 4
$G_{xy}\perp$ (MPa)	290	48	27	27
$G_{xy}\parallel$ (MPa)	430	170	120	110
Maximum capacity (g)	0.137	0.126	0.126	0.123
Displacement $\perp$ (m)	0.003	0.0064	0.0067	0.0071
Displacement $\parallel$ (m)	0.0012	0.0031	0.0039	0.0039

The graphs in Figure 23 show the convergence of the values of the shear modulus when the load is perpendicular ($G_{xy}\perp$) and parallel ($G_{xy}\parallel$) to the longitudinal axis of the beams. The difference for the maximum capacity between the third and fourth iteration is less than 3%.

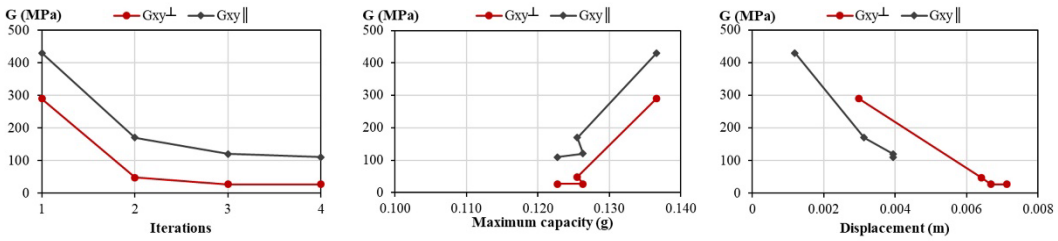

Figure 23 - Convergence of the values of the shear moduli of the 2D shell floors with steel beams.

The same methodology has been applied for the calculation of the shear moduli of the one-way floors with timber beams and ceramic tile vaults. The pushover capacity curves of the building with timber beam floors are presented in Figure 22b. The model with the orthotropic properties of the 2D shell floors estimated from the initial elastic stiffness of the 3D solid floors has the highest maximum capacity of 0.143g and presents the lowest

ductile behaviour. The ductility of the building increases by updating the elastic properties of the floors in the following iterations. Figure 24 presents the different iterations that have been done in order to obtain the final values of the shear modulus for both floor directions ($G_{xy\perp}$ and $G_{xy\parallel}$).

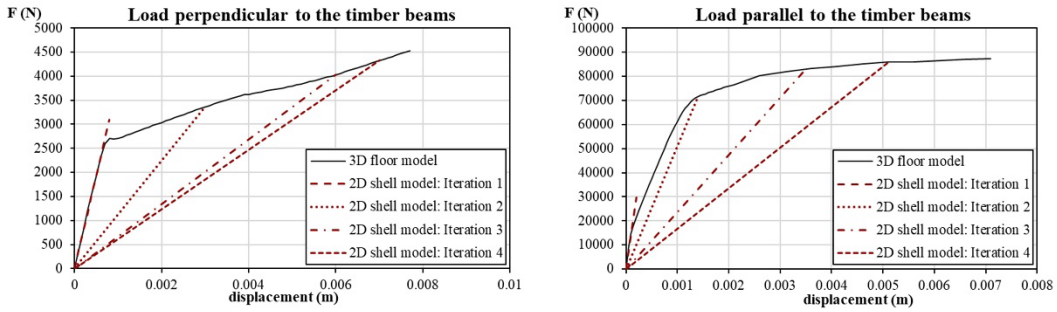

Figure 24 - Calibration of the effective shear stiffness of the 2D elastic shell model in the 3D building model: a) floors with timber beams parallel to the loading direction; b) floors with timber beams perpendicular to the loading direction.

Figure 25 shows the convergence of the values of the shear modulus for the floors with timber beams and ceramic tile vaults. Table 10 presents the values of the shear moduli, the maximum load capacity and corresponding relative displacements for the case of the timber beam floors. Again, the difference of the maximum capacity between the third and fourth iteration is smaller than 5%. The difference for the relative displacements of the floors with timber beams perpendicular to the loading direction is 12%. This confirms the convergence of the values of the orthotropic properties for the floors. The converged values of $G_{xy\perp}$ and $G_{xy\parallel}$ are 8.4% and 9.2% of the elastic ones considered in the first iteration.

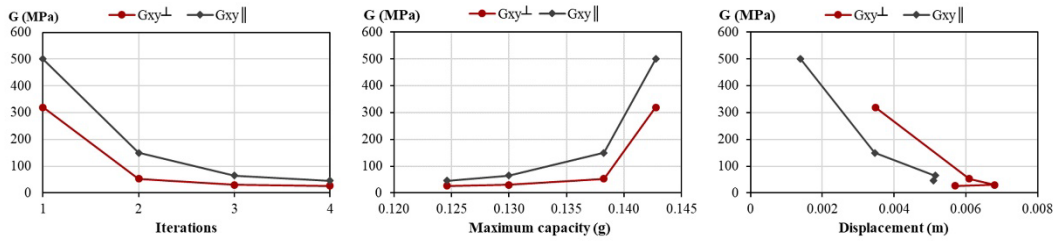

Figure 25 - Convergence of the values for the shear moduli of the 2D shell floors with timber beams.

Table 10 - Values obtained of the shear properties of the floor system with timber beams after the proposed iterative procedure

Convergence of the shear properties for the floors with timber beams				
Properties	Iteration 1	Iteration 2	Iteration 3	Iteration 4
$G_{xy\perp}$ (MPa)	320	53	30	27
$G_{xy\parallel}$ (MPa)	500	150	65	46
Maximum capacity (g)	0.143	0.138	0.13	0.125
Displacement ⊥ (m)	0.003	0.0061	0.0068	0.0057
Displacement ∥ (m)	0.0014	0.0035	0.0051	0.0051

6. Analysis and discussion of the results

After having calibrated the elastic orthotropic properties of the two studied floors, this section presents the results of the pushover analysis of the representative building with different floor systems.

Figure 26 shows the capacity curves of the static pushover analyses in terms of horizontal acceleration and displacement for the two analysed cases. The shape of the capacity curve is very similar for both cases. For the pushover analysis in the X direction, the FEM models present a linear behaviour until a sudden loss of stiffness, associated with the development of a soft-storey mechanism at the ground floor. This soft-storey mechanism

does not appear in the pushover analysis in the Y direction due to the presence of the transverse shear masonry walls, which are continuous along the whole height of the building. This difference makes the studied building more vulnerable in the X direction, showing lower load capacity, whereas a similar deformation capacity is obtained for both loading directions.

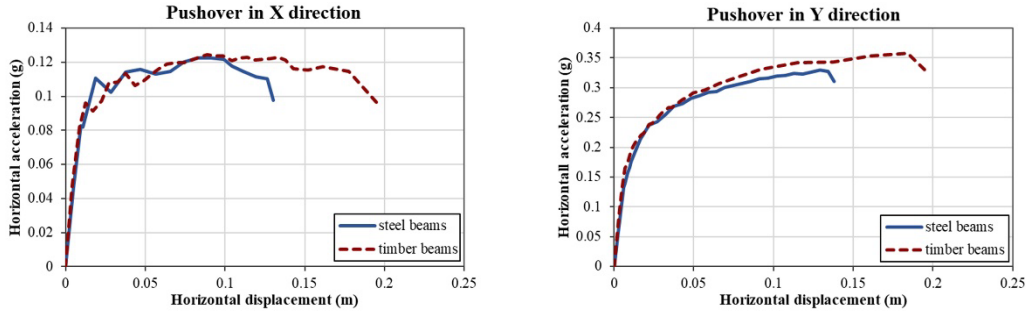

Figure 26 - Capacity curves of the Eixample building FEM model with the two different composite floor systems composed of steel or timber beams and tile vaults: pushover in X direction (left) and pushover in Y direction (right).

The maximum capacity in terms of the applied horizontal acceleration is very similar in both floor typologies for the pushover in the X direction. However, there is a difference of 8.3% for the maximum capacity of the pushover in the Y direction. A big difference exists in the deformation capacity, with the displacement reached at the last converged step of the analyses of the building with floors of steel beams being 33.5% and 29.5% lower than the one of timber beams for loading in X and Y directions, respectively. This shows a less ductile behaviour for the model with one-way floors of steel beams and tile ceramic vaults.

Figure 27 shows the capacity curves of the static pushover analyses in terms of base shear and horizontal displacement for the two floor systems with steel and timber beams, in the X and Y directions. As it can be seen from the graphs, there is no significant difference in stiffness between the two models with different floor systems. The total mass of the existing building with one-way floors of steel beams and masonry vaults is 1,572,300 kg and 1,369,500 kg for the model with floor system of timber beams and masonry vaults. Accordingly, the base shear capacity is higher in the model with floor systems composed of steel beams and masonry vaults than the model with timber beams, due to the difference in the mass of the floor systems.

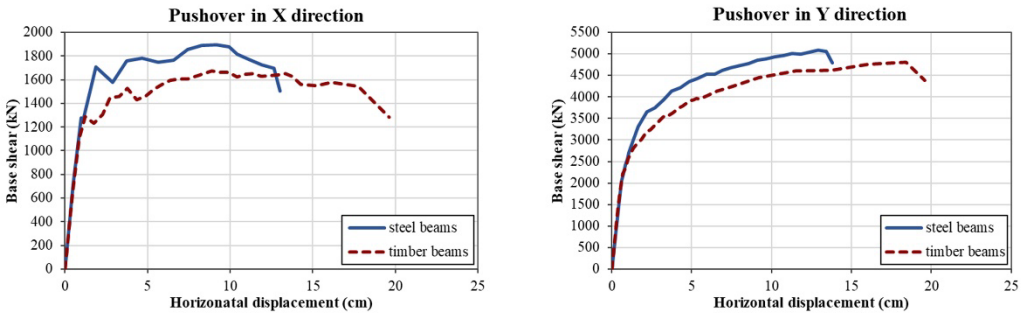

Figure 27 - Capacity curves in terms of base shear and horizontal displacements of the Eixample building FEM model with the two different composite floor systems composed of steel or timber beams and tile vaults: pushover in X direction (left) and pushover in Y direction (right).

As already mentioned, the difference in the horizontal stiffness observed between the X and Y axes of the building is attributed to the presence of big openings in the façades, while there is a small percentage of openings in the lateral walls and the lateral sides of the central core. The non-symmetrical distribution of openings between the front and rear façades has as important role in the seismic performance, producing a torsional response

when the structure is loaded towards the X direction. On the contrary, no torsional response is observed when loading along the Y direction, due to the symmetrical distribution of walls and openings in the Y axis of the building. The effect of the shear stiffness of the floors is more evident for loading along the X axis as discussed in the previous section.

Figure 28 and Figure 29 illustrate the damage localization simulated by the FE models in terms of maximum principal strains for the pushover analysis in X and Y direction, respectively.

With regard to the pushover in the X direction, the damage pattern is very similar for the two buildings with the different floors (Figure 28), with a formation of diagonal cracks in the piers of the front façade of the ground floors, which further leads to a shear failure. This type of mechanism is commonly known as soft-storey behaviour. The distribution of the tensile damage at the maximum capacity of the pushover analysis indicates a collapse mechanism of the piers of the front façade at the ground floor. Additionally, shear cracking appears in the other interior parts parallel to the façade and the lintels over the openings. Due to the absence of the interior walls at the ground floor in the frontal part of the structure and their replacement with steel beams, a local mechanism of overturning occurs at the lateral wall perpendicular to the seismic action. The level of the ground floor is seen as the weakest part of the structure because of the great change in the in-plane stiffness of the resisting elements.

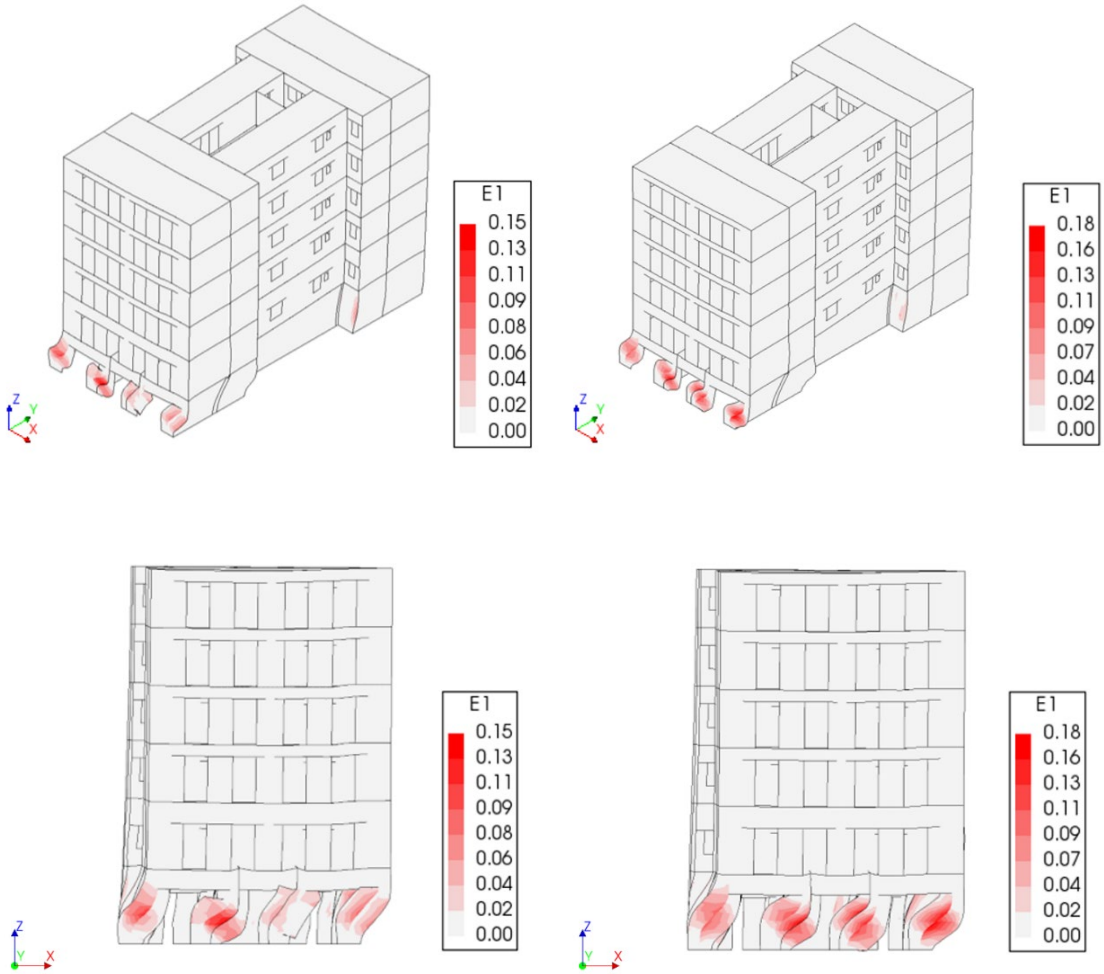

a) b)

Figure 28 - Contour of maximum principal strains at maximum capacity for pushover analysis in X direction: a) building with composite floor system consisting of steel beams and ceramic tile vaults; b) building with composite floor system consisting of timber beams and ceramic tile vaults. 3D view at the top and view of the front façade at the bottom.

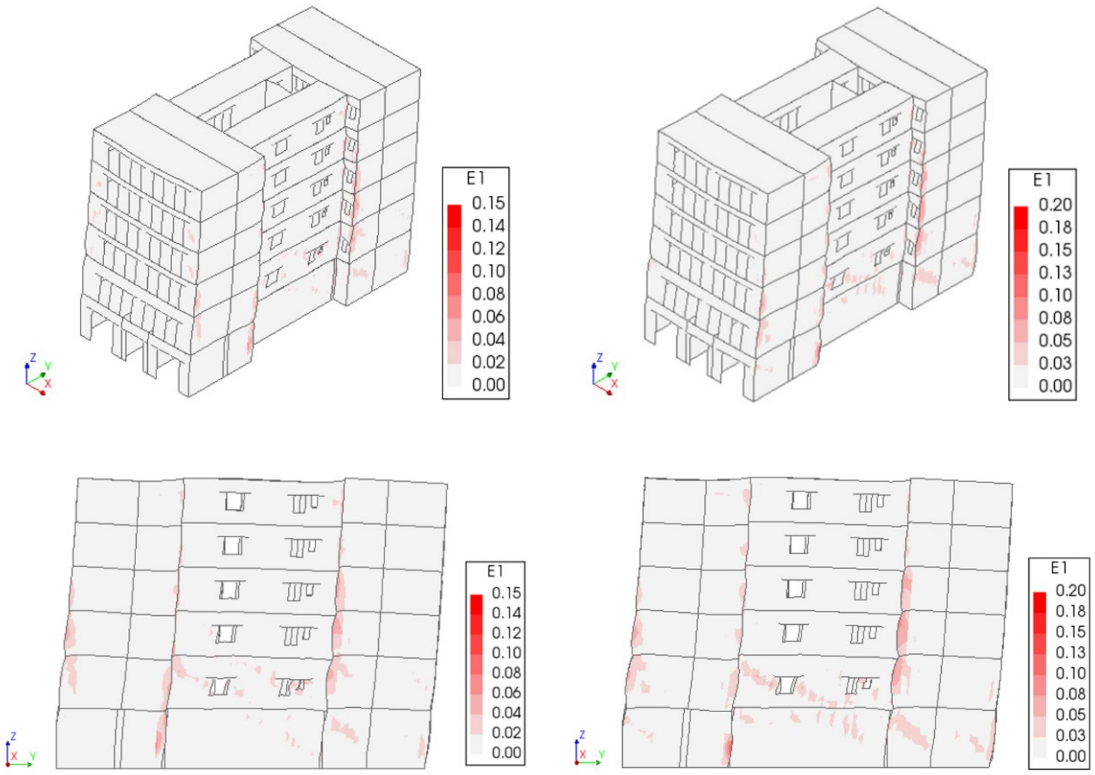

a) b)

Figure 29 - Contour of maximum principal strains at the maximum capacity for a pushover in Y direction: a) building with composite floor system of steel beams and tile vaults; b) building with composite floor system of timber beams and ceramic tile vaults. 3D view at the top and view of the lateral walls at the bottom.

The pushover analysis in Y direction shows a damage pattern symmetrical with respect to the Y axis, due to the symmetrical distribution of the resisting structural elements. Diagonal shear cracks appear on the lateral walls, starting from the lowest floor level, where the highest axial load exists, and progressing throughout the walls (Figure 29). Additionally, high levels of damage are observed in the corners of the semi-patios, which

have resulted in a vertical separation of the walls as a local mechanism. The damage pattern is very much alike for both models from the pushover in Y direction as well.

In conclusion, both one-way floors have similar behaviour for the seismic response of a multi-storey URM existing building. The collapse mechanism is the same for both types of floors, following the evolution of a soft-storey in the pushover in X direction and a shear failure of the lateral walls for the pushover in Y direction. The one distinction that should be noted is the variation in the displacement capacity, where the floors with timber beam present higher displacements than the ones with steel beams.

7. Conclusions

This paper has presented a procedure for the simplified and efficient modelling of jack arch one-way floors with tile vaults and steel or timber beams, which are a recurrent floor system in industrial and urban buildings of different countries. The adopted simplified modelling of floors consists in considering 2D shell elements with orthotropic elastic homogeneous material. The orthotropic properties have been computed adopting a novel iterative procedure, which updates the elastic parameters of the simplified linear 2D shell model until matching the in-plane seismic behaviour of a detailed nonlinear 3D floor model built with solid continuum finite elements. Once the simplified models for the floors are validated, they can be implemented in the global FEM model of selected URM building to evaluate its seismic assessment by means of a pushover analysis. A multi-storey URM building of the Eixample historical district in Barcelona has been considered as a case study.

The following conclusions can be drawn from the presented study:

- The proposed modelling procedure for composite floor systems with timber/steel beams and tile vaults constitutes a simplified and reliable methodology to calibrate the elastic material orthotropic properties of 2D shell diaphragms in a 3D building model.
- The calibrated elastic values of the orthotropic elastic properties can be used to represent the shear and axial stiffness of two different types of jack arch floors, i.e. including tile vaults and steel or timber beams. The procedure allows to accurately simulate their behaviour in case of the application of seismic actions.
- The proposed methodology has been applied to a case study, consisting in the analysis of a representative building of the Eixample district of Barcelona. Two different types of jack arch floors, one with timber and the second one with steel beams, showed similar results in terms of global stiffness, maximum capacity and collapse mechanisms. Differences exist in the maximum displacements, with the case of steel beams in the floors exhibiting lower displacement capacity and presenting a less ductile behaviour.
- The global seismic behaviour of the URM building changes by modifying the values of the elastic orthotropic properties used for the modelling of the floors as 2D shell elements in the 3D building model. The different in-plane stiffness influences both the capacity and the ductility of the existing URM buildings. Hence, the proper modelling of the shear stiffness of the different type of floors should be always carefully considered in the seismic assessment of existing URM masonry buildings.

- The buildings of the Eixample district present a very different response according to the loading direction. The presence of large open spaces in the ground-floor and a large number of openings in the front façade makes the structure more vulnerable for loading in the direction parallel to the façade. While this vulnerability is expected to be reduced due to the construction of these buildings in aggregates, the global behaviour is not expected to change as all structures share the same structural characteristics with the presence of a soft-storey at the ground floor. The maximum level of displacements reached by the structure is similar for loading parallel and orthogonal to the façade.

Acknowledgments

The authors gratefully acknowledge the financial support from the Ministry of Science, Innovation and Universities of the Spanish Government (MCIU), the State Agency of Research (AEI), as well as that of the ERDF (European Regional Development Fund) through the project SEVERUS (Multilevel evaluation of seismic vulnerability and risk mitigation of masonry buildings in resilient historical urban centres, ref. num. RTI2018-099589-B-I00). The first author gratefully acknowledges the AGAUR agency of the Generalitat de Catalunya for the financial support of her predoctoral grant.

8. References

[1] Senaldi I, Magenes G, Penna A, Galasco A, Rota M. The Effect of Stiffened Floor and Roof Diaphragms on the Experimental Seismic Response of a Full-Scale Unreinforced Stone Masonry Building. J Earthq Eng 2014;18:407–43.

https://doi.org/10.1080/13632469.2013.876946.

[2] Vintzileou E, Mouzakis C, Adami C-E, Karapitta L. Seismic behavior of three-leaf stone masonry buildings before and after interventions: Shaking table tests on a two-storey masonry model. Bull Earthq Eng 2015;13:3107–33. https://doi.org/10.1007/s10518-015-9746-x.

[3] Senaldi IE, Guerrini G, Comini P, Graziotti F, Penna A, Beyer K, et al. Experimental seismic performance of a half-scale stone masonry building aggregate. Bull Earthq Eng 2020;18:609–43. https://doi.org/10.1007/s10518-019-00631-2.

[4] Diaferio M, Foti D, Giannoccaro NI, Ivorra S. Optimal model through identified frequencies of a masonry building structure with wooden floors. Int J Mech 2014;8:282–8.

[5] Piazza M, Baldessari C, Tomasi R. The role in-plane floor stiffness in the seismic behaviour of traditional buildings. Proc. 14th World Conf. Earthq. Eng. Beijing, China, 12-17 Oct., Beijing: 2008.

[6] Ortega J, Saloustros S, Roca P. Seismic vulnerability assessment method for vernacular architecture considering uncertainty. In: Roca P, Pelá L, Molins C, editors. Int. Conf. Struct. Anal. Hist. Constr., Int. Cent. Numer. Methods Eng., Barcelona, Spain: CIMNE; 2021.

[7] Brignola A, Pampanin S, Podestà S. Evaluation and control of the in-plane stiffness of timber floors for the performance-based retrofit of URM buildings. Bull New Zeal Soc Earthq Eng 2009;42:204–21. https://doi.org/10.5459/bnzsee.42.3.204-221.

[8] Valluzzi M, Garbin E, Benetta MD, Modena C. In-plane strengthening of timber floors for the seismic improvement of masonry buildings. Proc. 11th World Conf. Timber Eng. WCTE, Trentino, Italy, 20 – 24 June, 2010.

[9] Giongo I. Role of the timber diaphragms in the seismic response of unreinforced masonry (URM) buildings. University of Trento, 2013.

[10] Lourenço PB, Mendes N, Ramos LF, Oliveira D V. Analysis of Masonry Structures Without Box Behavior. Int J Archit Herit 2011;5:369–82. https://doi.org/10.1080/15583058.2010.528824.

[11] ASCE/SEI 41-17. Seismic Evaluation and Retrofit of Existing Buildings. Reston, Virginia: American Society of Civil Engineers: Structural Engineering Institute; 2017.

[12] NZSEE. Assessment and improvement of the structural performance of buildings in earthquakes: prioritisation, initial evaluation, detailed assessment, improvement measures: recommen-dations of a NZSEE study group on earthquake risk buildings. Wellington: New Zealand Society for Earthquake Engineering Wellington, New Zealand; 2006.

[13] Paricio Casademunt A. Secrets d'un sistema constructiu: l'Eixample. Edicions U. Barcelona: Edicions de la Universitat Politècnica de Catalunya; 2001.

[14] Diodato M, Macchioni N, Brunetti M, Pizzo B, Nocetti M, Burato P, et al. Understanding Spanish Timber Jack Arch Floors : Examples of Assessment and Conservation Issues Understanding Spanish Timber Jack Arch Floors : Examples of Assessment and Conservation Issues. Int J Archit Herit 2015;9:641–54. https://doi.org/10.1080/15583058.2015.1041193.

[15] Maheri MR, Rahmani H. Seismic evaluation and design of jack arch slabs. Eng Struct 2003;25:1639–54.

[16] Maheri MR, Rahmani H. Static and seismic design of one-way and two-way jack arch masonry slabs. Proc 13th World Conf Earthq Eng Vancouver, Canada, 1-6 August 2004 2004;25:1639–54. https://doi.org/10.1016/S0141-0296(03)00143-3.

[17] Zahrai SM, Zahraei SA, Edalat Manesh R. Evaluation of retrofitting methods for flexible floor slab. Proc. First Eur. Conf. Earthq. Eng. Seism. Geneva, Switzerland, 3-8 Sept., Generva: 2006.

[18] Shakib H, Mirjalili A, Dardaei S, Mazroei A. Experimental Investigation of the Seismic Performance of Retrofitted Masonry Flat Arch Diaphragms. J Perform Constr Facil 2015;29:04014115. https://doi.org/10.1061/(asce)cf.1943-5509.0000611.

[19] Zahrai SM. Experimental study of typical and retrofitted jack arch slabs in a single story 3D steel building. Int J Civ Eng 2015;13.

[20] Pujades LG, Barbat AH, González-Drigo R, Avila J, Lagomarsino S. Seismic performance of a block of buildings representative of the typical construction in the Eixample district in Barcelona (Spain). Bull Earthq Eng 2012;10:331–49. https://doi.org/10.1007/s10518-010-9207-5.

[21] Gonzalez-Drigo R, Avila-Haro A, Barbat AH, Pujades LG, Vargas YF, Lagomarsino S, et al. Modernist unreinforced masonry (URM) buildings of barcelona: Seismic vulnerability and risk assessment. Int J Archit Herit 2015;9:214–30. https://doi.org/10.1080/15583058.2013.766779.

[22] Jiménez-Pacheco J, González-Drigo R, Pujades Beneit LG, Barbat AH, Calderón-

Brito J. Traditional High-rise Unreinforced Masonry Buildings: Modeling and Influence of Floor System Stiffening on Their Overall Seismic Response. Int J Archit Herit 2020. https://doi.org/10.1080/15583058.2019.1709582.

[23] FEMA 356. Prestandard and commentary for the seismic rehabilitation of buildings. Washington, USA: Federal Emergency Management Agency; 2000.

[24] Diodato M, Macchioni N, Brunetti M, Pizzo B, Nocetti M, Burato P, et al. A Peculiar Spanish Timber Floor, the "Revoltón": A Diagnostic Example at the "Palacio del Marqués de Benicarló." Adv Mater Res 2013;778:1064–71. https://doi.org/10.4028/www.scientific.net/AMR.778.1064.

[25] ITEC. Norma reglamentària d'edificació sobre accions en l'edificació en les obres de rehabilitació estructural dels sostres d'edificis d'habitatges. NRE-AEOR-93. Institut de Tecnología de la Construcció de Catalunya - ITEC; 1994.

[26] Casanovas X, Graus i Rovira R, Rosell JR. Manual de diagnosi i intervenció en sostres unidireccionals de formigó i ceràmics. Barcelona: Col·legi d'Aparelladors i Arquitectes Tècnics; 1993.

[27] Cornadó Bardón C. Comportament mecànic-estructural dels edificis històrics de murs d'obra de fàbrica de maó de l'Eixample de Barcelona. Universitat Politècnica de Catalunya, 2015.

[28] Dimovska S, Saloustros S, Pelà L, Roca P. Seismic vulnerability assessment of representative building typologies from Barcelona's Eixample district. In: Roca P, Pelá L, Molins C, editors. Int. Conf. Struct. Anal. Hist. Constr., Int. Cent. Numer. Methods Eng., Barcelona: CIMNE; 2021.

[29] DIANA FEA BV. DIsplacement method ANAlyser (DIANA FEA) User's Manual

release 10.4. Delft, Netherlands: 2020.

[30] CTE-DB-SE-M. Código Técnico de la Edificación. Documento Básico SE-M Seguridad Estructural: Madera. 2007.

[31] Mendes N, Lourenço PB. Sensitivity analysis of the seismic performance of existing masonry buildings. Eng Struct 2014;80:137–46. https://doi.org/10.1016/j.engstruct.2014.09.005.

[32] Aşıkoğlu A, Vasconcelos G, Lourenço PB, Pantò B. Pushover analysis of unreinforced irregular masonry buildings: Lessons from different modeling approaches. Eng Struct 2020;218. https://doi.org/10.1016/j.engstruct.2020.110830.

[33] Pereira JM, Correia AA, Lourenço PB. In-plane behaviour of rubble stone masonry walls: Experimental, numerical and analytical approach. Constr Build Mater 2021;271. https://doi.org/10.1016/j.conbuildmat.2020.121548.

[34] Chieffo N, Mosoarca M, Formisano A, Lourenço PB, Milani G. The effect of ground motion vertical component on the seismic response of historical masonry buildings: The case study of the Banloc Castle in Romania. Eng Struct 2021;249:113346. https://doi.org/https://doi.org/10.1016/j.engstruct.2021.113346.

[35] Segura J, Pelà L, Roca P, Cabané A. Experimental analysis of the size effect on the compressive behaviour of cylindrical samples core-drilled from existing brick masonry. Constr Build Mater 2019;228:116759. https://doi.org/10.1016/j.conbuildmat.2019.116759.

[36] MIT Ministerio delle Infrastrutture e del Transporti. Circolare del ministero delle

infrastructure e dei trasporti, n.7 del 21 Gennaio 2019: "Istruzioni per l'applicazione dell'aggiornamento delle Norme tecniche per le costruzioni di cui al D.M. 17 gennaio 2018. Cons. Super. Dei Lav. Pubblici. G.U. n.35 Del 11.02.2019; 2019.

[37] Lourenço PB. Recent advances in masonry modelling: micromodelling and homogenisation. Multiscale Model. Solid Mech. Comput. Approaches, vol. 3, 2008, p. 251–94.

[38] Turnsek V, Sheppard P. The shear and flexural resistance of masonry walls. Proc. Res. Conf. Earthq. Eng, Skopje: 1980.

[39] Moreno-González R, Bairán JM. Análisis del comportamiento sísmico de los edificios de obra de fábrica, típicos del distrito Eixample de Barcelona. Inf La Construcción 2011;63:21–32. https://doi.org/10.3989/ic.10.045.

[40] Endo Y, Llorens MS, Roca P, Pelà L. Dynamic Identification and Static Loading Tests of Timbrel Vaults: Application to a Modernist 20th Century Heritage Structure. Int J Archit Herit 2017;11:607–20. https://doi.org/10.1080/15583058.2016.1277566.

[41] Segura J, Pelà L, Roca P. Monotonic and cyclic testing of clay brick and lime mortar masonry in compression. Constr Build Mater 2018;193:453–66. https://doi.org/10.1016/j.conbuildmat.2018.10.198.

[42] Endo Y. Modelling and Structural analysis of historical masonry systems including vaulted structure. Universitat Politècnica de Catalunya, 2015.

[43] Campione G, Cavaleri L, Di Trapani F, Ferrotto MF. Frictional Effects in Structural Behavior of No-End-Connected Steel-Jacketed RC Columns :

Experimental Results and New Approaches to Model Numerical and Analytical Response. J Structiral Eng 2017;143. https://doi.org/10.1061/(ASCE)ST.1943-541X.0001796.

[44] PCI Industry Handbook Committee. PCI Design Handbook: Precast and Prestressed Concrete. 2004.

[45] de la Fuente-Leon J, Lafuente-Jimenez E, Hermosilla D, Broto-Cartagena M, Gasco A. Physico-mechanical properties of Spanish juniper wood considering the effect of heartwood formation and the presence of defects and imperfections. For Syst 2014;23:64–71. https://doi.org/10.5424/fs/2014231-03671.

[46] Aira JR, Arriaga F, Íñiguez-González G, Crespo J. Static and kinetic friction coefficients of Scots pine (Pinus sylvestris L.), parallel and perpendicular to grain direction. Mater Construcción 2014;64:e030. https://doi.org/10.3989/mc.2014.03913.

[47] Adam JM, Ivorra S. Behaviour of axially loaded RC columns strengthened by steel angles and strips. Steel Compos Struct 2007;7:405–419. https://doi.org/10.12989/scs.2007.7.5.405.

[48] LEMPRIERE BM. Poisson's ratio in orthotropic materials. AIAA J 1968;6:2226–7. https://doi.org/10.2514/3.4974.